

¹ **High-resolution regional climate model evaluation using variable-resolution**

² **CESM over California**

³ Xingying Huang, * Alan M. Rhoades and Paul A. Ullrich

⁴ *Department of Land, Air and Water Resources, University of California, Davis*

⁵ Colin M. Zarzycki

⁶ *National Center for Atmospheric Research*

⁷ *Corresponding author address: Xingying Huang, Department of Land, Air and Water Resources,

⁸ University of California Davis, Davis, CA 95616.

⁹ E-mail: xyhuang@ucdavis.edu

ABSTRACT

10 Understanding the effect of climate change at regional scales remains a
11 topic with intensive researches. Due to computational constraints, high hor-
12 izontal resolutions required to reach regional scales have been largely out of
13 reach for current global climate models. However, high resolution is needed
14 to represent fine-scale processes and topographic forcing, which is a signif-
15 icant driver of local climate variability. Although regional climate models
16 (RCMs) have been widely used at these scales, variable-resolution global cli-
17 mate models (VRGCMs) have arisen as an alternative for studying regional
18 weather and climate. In this paper, the recently developed variable-resolution
19 option within the Community Earth System Model (CESM) is assessed for
20 long-term regional climate modeling. The mean climatology of temperature
21 and precipitation, across California's diverse climate zones, is analyzed and
22 contrasted with the Weather Research and Forcasting (WRF) model (as a tra-
23 ditional RCM), regional reanalysis, gridded observational datasets and a uni-
24 form high-resolution CESM with the finite volume (FV) dynamical core. The
25 results show that variable-resolution CESM is competitive in representing re-
26 gional climatology on both annual and seasonal time scales. This assessment
27 adds value to the use of VRGCMs for projecting climate change over the
28 coming century and improve our understanding of both past and future re-
29 gional climate related to fine-scale processes. This assessment is also relevant
30 for addressing the scale limitation of current RCMs or VRGCMs when next-
31 generation model resolution increases to $\sim 10\text{km}$ and beyond.

³² **1. Introduction**

³³ Global climate models (GCMs) have been widely used to simulate both past and future cli-
³⁴ mate. Although GCMs have demonstrated the capability to successfully represent large-scale
³⁵ features of the climate system, they are usually employed at coarse resolutions ($\sim 1^\circ$), largely
³⁶ due to computational limitations. Global climate reanalysis datasets, which assimilate climate
³⁷ observations using a global model, represent a best estimate of historical weather patterns, but
³⁸ still have relatively low resolutions no finer than 0.5° (<http://reanalyses.org/atmosphere/>
³⁹) overview-current-reanalyses). Consequently, regional climate is not well captured by ei-
⁴⁰ ther GCMs or global reanalysis datasets. However, dynamical processes at unrepresented scales
⁴¹ are significant drivers for regional and local climate variability, especially over complex terrain
⁴² (Soares et al. 2012). In order to capture these fine-scale dynamical features, high horizontal reso-
⁴³ lution is needed to allow for a more accurate representation of fine-scale forcings, processes and
⁴⁴ interactions (Leung et al. 2003a; Rauscher et al. 2010). With these enhancements, the regional
⁴⁵ climate information is expected to be more usable for policy makers and local stakeholders in
⁴⁶ formulating climate adaptation and mitigation strategies.

⁴⁷ In order to model regional climate at high spatial and temporal resolution over a limited area,
⁴⁸ downscaling methods have been developed. There are largely two approaches for downscaling
⁴⁹ including statistical downscaling and dynamical downscaling. Dynamical downscaling is popu-
⁵⁰ lar and commonly employed using nested limited-area models (LAMs) or by applying a variable
⁵¹ resolution GCM (VRGCM) to model regional scales (Laprise 2008). In this context, LAMs are
⁵² typically referred as regional climate models (RCMs) when applied to climate scales. Forced by
⁵³ output of GCMs or reanalysis data, RCMs have been widely used, particularly to capture physi-
⁵⁴ cally consistent regional and local circulations at the needed spatial and temporal scales (Leung

55 et al. 2003a; Christensen et al. 2007; Bukovsky and Karoly 2009; Mearns et al. 2012). Recently,
56 VRGCMs have been increasingly employed for modeling regional climate. This approach uses
57 a global model that includes high-resolution over a specific region and coarse resolution over the
58 remainder of the globe (Staniforth and Mitchell 1978; Fox-Rabinovitz et al. 1997). And there are
59 different strategies to achieve high-resolution over the area of interest such as stretched-grid mod-
60 els or grid refinement technique (Fox-Rabinovitz et al. 1997; Ringler et al. 2008; Skamarock et al.
61 2012). VRGCMs have been demonstrated to be effective for regional climate studies and appli-
62 cations at a reduced computational cost compared to uniform GCMs (Fox-Rabinovitz et al. 2001,
63 2006; Rauscher et al. 2013; Zarzycki et al. 2015). Fox et al. (2000) found that the stretched-grid
64 version of a GCM captured not only large-scale meteorological patterns as traditional GCMs did
65 but also mesoscale features especially when considering orographic forcing (Fox-Rabinovitz et al.
66 2000).

67 Compared with RCMs, a key advantage of VRGCMs is that they use a single, unified modeling
68 framework, rather than a separate GCM and RCM. Thus, VRGCMs avoid potential inconsistency
69 between the global and regional domains, and naturally support two-way interaction between these
70 domains without the need for nudging (Warner et al. 1997; McDonald 2003; Laprise et al. 2008;
71 Mesinger and Veljovic 2013). However, in order to obtain deeper insight into the performance
72 of these two modeling approaches, it is necessary to compare them directly. For the purposes of
73 this paper, we will focus on the recently developed variable-resolution Community Earth System
74 Model (varres-CESM) using the grid refinement technique as our VRGCM of interest. Although
75 CESM has been well-used for uniform resolution modeling, variable-resolution in the Commu-
76 nity Atmosphere Models (CAM) Spectral Element (SE) dynamical core has only been recently
77 developed. Zarzycki et al. (2014) applied this option in CAM-SE and showed that high-resolution
78 simulation of topical cyclones represented significant improvements over the unrefined simula-

79 tion. Zarzycki et al. also compared the large-scale features of varres-CESM 0.25° and uniform
80 CESM at one degree, and found that adding refined region over the globe did not affect the global
81 circulation noticeably (Zarzycki and Jablonowski 2014; Zarzycki et al. 2015).

82 However, varres-CESM has yet to be rigorously investigated for long-term regional climate sim-
83 ulation (Taylor and Fournier 2010; Zarzycki et al. 2014). And in this paper, it is the first time to
84 investigate whether VRGCMs can show similar or even better ability in regional climate modeling
85 compared with traditional method of RCMs. The goal of this paper is to evaluate the perfor-
86 mance of varres-CESM against gridded observational data, reanalysis data and in comparison to a
87 RCM. Also, outputs from a uniform high-resolution CESM simulation have also been utilized here
88 (Wehner et al. 2014a). Our variable-resolution simulations will focus on relatively high resolutions
89 for climate assessment, namely 28km and 14km grid spacing, which are much more typical for
90 dynamically downscaled studies. For comparison with the more widely used RCM method, the
91 Weather Research and Forecasting (WRF) model will be applied at 27km and 9km grid spacing
92 (Skamarock et al. 2005). The study focuses on models' ability to represent current climate statis-
93 tics, particularly those relative to climate extremes. We anticipate that this assessment will add
94 value in modeling mean regional climatology and improve our understanding about the effects of
95 multi-scale processes in regional climate regulation. Our goal is also to advance the understanding
96 of better use of models in future climate predictions and climatic extremes studies regionally.

97 In this paper, we use California (CA) as our study area. With its complex topography, coastal
98 influences, and wide latitudinal range, this makes CA an excellent test bed. Also, an understanding
99 of local climate variability is incredibly important for policymakers and stakeholders in California
100 due to its vast agricultural industry, wide demographics, and vulnerability to anthropogenically-
101 induced climate change (Hayhoe et al. 2004; Cayan et al. 2008). RCM simulations over California
102 have also been conducted in previous studies and showed the need of high resolution to better

103 study regional climate and extreme events, especially over complex topography with large climate
104 gradients (Leung et al. 2004; Kanamitsu and Kanamaru 2007; Caldwell et al. 2009; Pan et al. 2011;
105 Pierce et al. 2013). Caldwell et al. (2009), in particular, presented results from WRF (Weather
106 Research and Forecasting) at 12km spatial resolution showing both the overall consistency and
107 some biases (e.g. overestimation of precipitation) between simulations and observations.

108 This paper is organized as follows. Section 2 describes the model setup, verification data and
109 evaluation methods. In section 3, results are demonstrated focusing on 2 m temperature (Ts) and
110 precipitation (Pr). Key results are summarized along with further discussion in section 4.

111 **2. Models and Methodology**

112 *a. Simulation design*

113 All simulations use the AMIP (Atmospheric Model Intercomparison Project) protocols (Gates
114 1992). AMIP simulations attempt to recreate a climatology similar to that observed over the past
115 few decades, with prescribed sea-surface temperatures (SSTs) and ice concentrations.

116 1) VARRES-CESM

117 CESM is a state-of-the-art Earth modeling framework developed by the National Center for At-
118 mospheric Research (NCAR), consisting of atmospheric, oceanic, land and sea ice components
119 and has been heavily used for understanding the effects of global climate change (Neale et al.
120 2010a; Hurrell et al. 2013). Different component models are connected by a couple component.
121 In this way, the interfacial states and fluxes between the various component models are commu-
122 nicated and the fluxed quantities are conserved. Since we follow AMIP protocols in this study,
123 communication is mainly occurred between atmospheric and land model. Ocean model and sean
124 ice component are disabled. Here, CAM version 5 (CAM5) (Neale et al. 2010b) and the Com-

125 munity Land Model (CLM) version 4 (Oleson et al. 2010) are used. As mentioned earlier, SE
126 was used as the dynamical core in CAM along with the variable-resolution grid support. The
127 FAMIP5 (F_AMIP_CAM5) compset was chosen for the simulations as it is the standard protocol
128 for AMIP and is less computationally demanding.

129 For our study, the variable-resolution cubed-sphere grids are generated for use in CAM and CLM
130 with the open-source software package SQuadGen (Ullrich 2014). The grids used are depicted in
131 Figure 1. The maximum horizontal resolution on these grids are 0.25 degree ($\sim 28\text{km}$) and 0.125
132 degree ($\sim 14\text{km}$) respectively, with one degree resolution covering the rest of the globe. These
133 resolutions have been selected because CAM-SE naturally supports a 2:1 aspect ratio, meaning
134 there are two transition layers from 1 degree to 0.25 degree, and one additional transition from
135 0.25 degree to 0.125 degree. The meteorological patterns (e.g. wind, pressure and precipitation)
136 showed natural and conserved results over the transition boundary as described in (Zarzycki et al.
137 2015). The time period is from 1979-01-01 to 2005-12-31 (UTC), and year 1979 was discarded as
138 spin up time for CLM4.0. We chose this time period to present the recent historical climate and try
139 to achieve the best balance between reproducibility and computational feasibility, which is further
140 discussed in the Methodology part.

141 Variable-resolution topography files have been produced by starting with the National Geophys-
142 ical Data Center (NGDC) 2-min ($\sim 3.5\text{ km}$) Gridded Global Relief Dataset (ETOPO2v2) topog-
143 raphy dataset and applying the differential smoothing technique by adjusting the c parameter from
144 Eq. (1) in Zarzycki et al. (2015). The grid-scale topography is showed in Figure 3. The higher
145 resolution simulations provide a much finer representation of regional topography. This is impor-
146 tant for understanding local climate since topography is an important driver for fine-scale dynamic
147 processes, especially over complex terrain.

148 Land surface datasets, and plant functional types, were created at the standard 0.50 degree res-
149 olution. Initialized conditions are provided for both CAM and CLM. Greenhouse gas (GHG)
150 concentrations are prescribed based on historical observations. SSTs and ice coverage are sup-
151 plied by the one degree Hadley Centre Sea Ice and Sea Surface Temperature dataset (HadISST)
152 (Hurrell et al. 2008). Tuning parameters are not modified from their default configuration.

153 2) UNIFORM CESM

154 Output from a globally uniform CESM run at 0.25° spatial resolution is utilized for comparison.
155 It helps us to see if variable-resolution CESM, which is at much lower computation cost than
156 uniform one, can show comparable performance in modeling mean climatology (Bacmeister et al.
157 2014). This globally uniform simulation uses the CAM5-FV (finite volume) dynamical core and
158 is described in additional detail in Wehner et al. (2014a) and Wehner et al. (2014b). **need to add**
159 **details about this and which parameters are different from the public version.**

160 3) WRF

161 WRF has gained wide acceptance in studying regional climate over the past decade, showing
162 its adequate capability in representation of fine-scale climate properties (Lo et al. 2008; Leung
163 and Qian 2009; Soares et al. 2012). In this study, the fully compressible non-hydrostatic WRF
164 model in version 3.5.1 with the Advanced Research WRF (ARW) dynamical solver is used. ERA
165 (ECMWF re-analysis)-Interim data at surface and pressure-level was used to provide initial and
166 lateral conditions for the domains. The lateral conditions and SSTs were updated every 6 hours.
167 ERA-Interim reanalysis (~ 80 km) has been widely used and validated for its reliability as forcing
168 data (Dee et al. 2011). Two simulations are conducted with finest horizontal resolution of 27km
169 and 9km respectively, over the same time period as varres-CESM. The ~ 10 km resolution is

170 actually finer than most previous studies for long-term climate. Also, the year 1979 is used as a
171 spin-up period and is discarded for purposes of analysis.

172 The simulation domains of WRF are depicted in Figure 2. For the WRF 27km simulation,
173 one domain is used. For the WRF 9km simulation, two nested domains are used with the outer
174 domain at 27km (same as the WRF 27km) and inner domain at 9km horizontal grid resolution,
175 satisfying the natural WRF refinement ratio of 3:1. As a common way in WRF, two-way nesting
176 is enabled by feeding back information from the fine grid onto the coarse grid, thus the nested
177 region's process of the coarse domain is replaced by the fine grid result (Skamarock and Klemp
178 2008). Both grids are centered on CA and have respectively, 120×110 and 151×172 grid points.
179 Around the boundaries, 10 grid points are used as lateral relaxation zones. In order to reduce
180 the drift between forcing data and RCM, grid nudging (Stauffer and Seaman 1990) was applied
181 to the outer domain every 6 hours at all levels except the planetary boundary layer (PBL) as
182 suggested by Lo et al. (2008). This setup uses 41 vertical levels with model top pressure at 50
183 hPa. The topography data used in 27km and 9km are interpolated from USGS (U.S. Geological
184 Survey) elevation data with 10m and 2m resolution respectively. The grid-scale topography is
185 contrasted in Figure 3. Some differences are also apparent between the 28km varres-CESM and
186 27km WRF model, particularly over the Central Valley, and indicative of a different methodology
187 for preparation of the topography dataset.

188 Additionally, we used the following physics parameterizations: WSM (WRF Single-Moment)
189 6-class graupel microphysics scheme (Hong and Lim 2006), Kain-Fritsch cumulus scheme (Kain
190 2004), CAM shortwave and longwave radiation schemes (Collins et al. 2004). These settings
191 are supported by the one-year test running result with different options of cumulus scheme and
192 radiation schemes. For the boundary layer, the Yonsei University scheme (YSU) (Hong et al.
193 2006) and the Noah Land Surface Model (Chen and Dudhia 2001) were used. Both were chosen

¹⁹⁴ as they are common for climate applications that balance long-term reliability and computational
¹⁹⁵ cost.

¹⁹⁶ *b. Datasets*

¹⁹⁷ For validation purpose, available reanalysis and gridded observational datasets of the highest
¹⁹⁸ quality are employed (see Table 1). Although gridded observational datasets are generally based
¹⁹⁹ on measurements of weather stations, they are based on different network of stations. And these
²⁰⁰ datasets are scaled and gridded using varied interpolation techniques, elevation models and pro-
²⁰¹ cessing algorithms. In this way, using multiple reference datasets rather than one is important
²⁰² to account for the uncertainties, when assessing the performance of the WRF and CESM simu-
²⁰³ lations in terms of both mean behavior and variability. Moreover, in this study, our purpose of
²⁰⁴ using these products is to serve as realistic proxies to allow for a comparison of the model results.
²⁰⁵ We acknowledge that reanalysis products are particularly sensitive to model choice and choice of
²⁰⁶ assimilated observations and so cannot be treated as truth. Detailed descriptions of these datasets
²⁰⁷ are as follows.

²⁰⁸ (i) *NARR*: The North American Regional Reanalysis (NARR) provides dynamically downscaled
²⁰⁹ data over North America at ~ 32 km resolution and 3 hourly intervals from 1979 through present
²¹⁰ (Mesinger et al. 2006). It is National Centers for Environmental Prediction (NCEP)'s high reso-
²¹¹ lution reanalysis product. All major climatological variables are present in NARR, making it an
²¹² excellent candidate for assessment of regional climate. Nonetheless, some inaccuracies have been
²¹³ identified in NARR that must be accounted for, including deficiencies in precipitation fields away
²¹⁴ from the continental US (Bukovsky and Karoly 2007).

215 (ii) *NCEP CPC*: This data set is CPC unified gauge-based analysis of daily precipitation pro-
216 vided by the National Oceanic and Atmospheric Administration (NOAA) Climate Prediction Cen-
217 ter (CPC). It is a suite of unified precipitation products with consistent and improved quality by
218 combining all information available at CPC and by taking advantage of the optimal interpolation
219 (OI) objective analysis technique. The gauge analysis covers the Conterminous United States with
220 a fine-resolution at 0.25° from 1948/01/01 to 2006/12/3.

221 (iii) *UW*: The UW daily gridded meteorological data is obtained from the Surface Water Mod-
222 eling group at the University of Washington (Maurer et al. 2002; Hamlet and Lettenmaier 2005).
223 UW incorporated topographic corrections by forcing the long-term average precipitation to match
224 that of the PRISM dataset. Temperature dataset is produced in a similar fashion as precipitation,
225 but used a simple 6.1 K/km lapse rate for topographic effect. The dataset is at 0.125° horizontal
226 resolution and provided from year 1949 to 2010.

227 (iv) *PRISM*: The Parameter-elevation Regressions on Independent Slopes Model (PRISM) (Daly
228 et al. 2008) supports a 4km gridded dataset obtained by taking wide range of point measurements
229 and applying a weighted regression scheme that accounts for many factors affecting the local cli-
230 matology. The datasets include total precipitation and minimum/maximum, (derived) mean tem-
231 peratures and dewpoints, based on sophisticated quality control measures. Monthly climatological
232 variables are available for 1895 through 2014 provided by the PRISM Climate Group. PRISM is
233 U.S. Department of Agriculture (USDA)'s official climatological data. We will use this product as
234 the main reference dataset for model assessment.

235 (v) *Daymet*: Daymet is an extremely high resolution (1 km) gridded dataset with daily outputs
236 of total precipitation, humidity, and minimum/maximum temperature covering the years of 1980
237 through 2013 (Thornton et al. 1997; Thornton and Running 1999; Thornton et al. 2000). The

²³⁸ dataset is produced using an algorithmic technique that ingests point station measurements in
²³⁹ conjunction with a truncated Gaussian weighting filter. Some adjustments are made to account for
²⁴⁰ topography. Daymet is available through the Oak Ridge National Laboratory Distributed Active
²⁴¹ Archive Center (ORNL DAAC).

²⁴² *c. Methodology*

²⁴³ Near surface (2 meter) temperature and precipitation have been analyzed over California, to
²⁴⁴ assessing the models' performances in representing the mean climatology. Specifically, evaluation
²⁴⁵ focuses on daily maximum, minimum and average 2m temperatures (Tmax, Tmin and Tavg), and
²⁴⁶ daily precipitation (Pr). These variables are key for a baseline climate assessment, particularly
²⁴⁷ for their relationship with water resources, agriculture and health. With the overall warm climate
²⁴⁸ and large impact of heat waves over CA, we focus on the summer season covering June, July and
²⁴⁹ August (JJA) in the aspect of temperature. Since the vast majority of precipitation in CA occurs
²⁵⁰ in the winter season, together with the accumulation of snowpack, in this way, precipitation over
²⁵¹ December-January-February (DJF) is emphasized.

²⁵² In order to adequately account for natural variability even at regional scale, simulations need to
²⁵³ be run long enough (Solomon 2007). However, there is no particular timeframe for climatology
²⁵⁴ studies. Average weather conditions over 30-year or so are typically used to track climate to make
²⁵⁵ sure that the data is long enough to calculate an average that is not influenced by year-to-year
²⁵⁶ variability (Dinse 2009). In this study, 26-year current-climate runtime is chosen to reasonably
²⁵⁷ balance the reproducibility and computational availability. We have studied the variability of mean
²⁵⁸ temperature and precipitation in both simulations and observations over 5, 10, 20 and 25 seasons
²⁵⁹ or years, and the results showed that 20 or 25 years' simulation are long enough to adequately

260 capture the regionally climate variability. 30 years or longer run time may sound better, but are
261 not necessary for our case.

262 All the results showed in the following part are based on the time period from year 1980 to 2005.
263 All the datasets have been investigated first to see if time trend exists over this 26 years period, and
264 the least squares linear trend has been removed from original datasets if existing. It is found that
265 for temperature, there do have statistically significant linear trend over some parts of CA under the
266 two-tailed t-statistic significance level of 0.05. However, no significant trend has been detected for
267 precipitation.

268 Further, in order to better assess the treatment of California's varied climate regions, the state
269 has been divided into five regional zones, including: the Central Valley, Mountain Region, North
270 Coast, South Coast, and Desert Region as showed in Figure 2. The division of these five zones
271 are loosely based on the results of Abatzoglou et al. (2009) and the building climates zones from
272 California Energy Commission. For parts of the results analyses, simulations and datasets are
273 masked to restrict climate variables to specific zones. We aim to examine the statistics of data
274 averaged over geographic climate zones instead of just on grid-cell analysis.

275 Statistical measurements have been used to quantify the performances of the models comparing
276 with the reference datasets. These statistical variables include the Root-mean-square deviation
277 (RMSD), mean absolute difference (MAD), mean relative difference (MRD) and correlation, and
278 sample standard deviation.

279 When calculating the difference at grid point, the reference datasets are remapped to the given
280 model's output resolution. Datasets are remapped using a bilinear interpolation method, which
281 has been verified to provide satisfactory performance. Other remapping algorithms, such as patch-
282 based have been tested and do not exhibit notable differences.

283 Student's t-test is used when necessary to see if two sets of yearly or seasonally averaged data are
284 significantly different from each other, and 0.05 is used as critical levels of significance. We need
285 to point out that this is just a approximate test to further support our results analysis since the two
286 populations being compared should follow a normal distribution.

287 **3. Results**

288 *a. Temperature*

289 The mean JJA Tmax, Tmin and Tavg climatology over 26 years of simulations together with
290 PRISM are shown in Figure 4. The statistical measurements over whole CA area are showed in
291 Table 2. We can see that all simulations have captured the spatial climate patterns showed by
292 the PRISM, with high spatial correlations (>0.95), especially for Tmax and Tavg. For Tmax,
293 comparing with reference datasets, varres-CESM showed a warmer climate generally with about
294 2 to 3°C difference. Uniform CESM is similar as varres-CESM, but with a larger RMSD value
295 ($\sim 4^{\circ}\text{C}$). However, WRF output displayed overall colder climate, especially the WRF 9km, with
296 about 2 to 3°C difference. Tmax over Central Valley has been overestimated by all the simulations
297 and the possible reason has been discussed at the end of this part.

298 For Tmin, varres-CESM still showed a warm effect (~ 3 to 4°C), with a particularly egregious
299 overestimation over Nevada. WRF also had overall warm effect but displayed better performance
300 than varres-CESM with smaller differences (~ 2 to 3°C), comparing with reference datasets. How-
301 ever, the pattern of Tmin presented in Figure 4 in both WRF simulations suggests a cooler interior
302 to the Central Valley and warmer perimeter, which is not supported by observations. Overestima-
303 tion of Tmin and Tmax by varres-CESM leads a similar overestimation for Tavg, so does uniform
304 CESM. And underestimation of Tmax by WRF, causes a underestimation for Tavg, but still sta-

tistically more close to reference datasets than CESMs. The sample standard deviations of the
305 JJA Tmax, Tmin and Tavg by models and PRISM are showed in Figure 5. It can be seen that the
306 variability has little changes across difference sub-zones, and the values are around 0.5 to 1.5 °C
307 for all the datasets, except some higher values ($\sim 2^{\circ}\text{C}$) over mountains regions in WRF 9km.
308

309 There are some minor uncertainties, as we already discussed, showed when comparing with
310 different reference datasets. We have made the Student's t-test to see if the JJA Tmax, Tmin and
311 Tavg from PRISM, UW and Daymet are statistically different from each other. And the results
312 showed that they are the same at the significance level of 0.05 over most regions of our study
313 area, except coastal regions. These observations are still of the highest quality available and the
314 uncertainty is relatively small compared with difference from the simulations, thus are unlikely
315 impacting the evaluation results.

316 Overall, varres-CESM 0.125 degree performed best in simulating long-term Tmax, and WRF is
317 better at modeling Tmin than varres-CESM. When comparing against NARR (not showed), the
318 overestimation of Tmin are largely reduced for varres-CESM. This suggests that the source of the
319 temperature bias in varres-CESM and NARR may be related. Additionally, there are a positive
320 2 K SST bias near the California coastline between varres-CESM and WRF runs. This may also
321 cause overestimation of temperatures. The sea breeze effect, associated with cooler temperatures
322 near the San Francisco Bay, are apparent in all runs. It is especially encouraging that differences in
323 the varres-CESM simulations, which only used prescribed SSTs, closely matched those of WRF,
324 which were forced at the lateral domain boundaries with reanalysis data.

325 The seasonal cycle of Tavg is shown in Figure 6 for simulations and reference data from PRISM
326 and NARR. The models do show good consistency with reference data with no larger than 2°C
327 difference, which mainly occurred in the coldest and hottest seasons. Compared with PRISM,
328 Varres-CESM showed positive difference over the summer season in all sub-zones except coastal

329 regions, and negative difference over winter season in all zones, indicating larger temperature
330 range. The uniform CESM is similar to varres-CESM, with about 1°C larger difference. WRF
331 has better performance in presenting the monthly trend than CESM with about 1°C underestima-
332 tion over all seasons. No notable differences can be discerned when comparing models across
333 resolutions.

334 The variability over each month is expressed by the sample standard deviation showed in Figure
335 7. Generally, local variability of Tavg is under 3°C , mostly within the range from 1 to 2°C . Among
336 the simulations, WRF 27km is most consistent with PRISM. WRF 9km is also close to PRISM,
337 but has $\sim 1^{\circ}\text{C}$ larger variability over January and February. Varres-CESM basically showed about
338 0.5°C more scattered values (either above or lower) comparing to reference datasets, and uniform
339 CESM has about 0.5°C lower variability than PRISM.

340 For the temperature climatology in California, we are most interested in the Tmax over summer
341 season due to the impact of summer heat waves. We depict the frequency distribution of Tmax
342 using all the JJA daily values over 26 years. The results of the simulations and reference datasets
343 of Daymet and UW are showed in Figure 8. Properties of the frequency distribution, including
344 average, variability, skewness and Kurtosis are tabulated in Table 3. Though with some deviations,
345 similar distribution shapes with tails off to left are present for both models and observations.
346 Contrasting with WRF, varres-CESMs are more close to reference datasets. WRF 9km tended to
347 be colder. Models including varres-CESM and WRF 27km are more consistent with observations
348 for higher values than the peak and less consistent at lower values. For representation of heat
349 extremes, both varres-CESM and WRF 27km exhibit satisfactory performance over most regions
350 except in Central Valley (CV). No obvious improvement is associated with higher resolution in
351 varres-CESM.

352 In the Central Valley, models show a clear warm effect and associated long tail, with tempera-
353 tures reaching near 50°C. As discussed before, all models do overestimate Tmax over CV. In order
354 to further assess the accuracy of the gridded observations, we examine the Tmax data directly from
355 recorded weather station observations over the CV. The results validate that Tmax values above
356 45°C are rare (although station observations suggest these days may be slightly more frequent than
357 suggested by UW and Daymet). The warm bias associated with the aforementioned extreme hot
358 days in both varres-CESM and WRF is likely correlated with overly dry summertime soil moisture,
359 as discussed in Caldwell et al. (2009). This could be caused by the lack of accurate land surface
360 treatment in climate models. areas. Bonfils and Lobell (2007) found that irrigation in Central Val-
361 ley has significantly decreased summertime maximum temperatures especially in heavily-irrigated
362 areas (Bonfils and Lobell 2007). Other studies have also found the cooling effects of irrigation,
363 such as (Kueppers et al. 2007).

364 *b. Precipitation*

365 California is known for the shortage of natural water resources with extreme drought over sum-
366 mer season. In this way, the winter season is particularly important for California as it accounts
367 for 50 percent of the ~22.5 inches that California receives for its total annual average precipitation
368 amounts (<http://www.ncdc.noaa.gov/cag/>).

369 The long-term average climatologies of DJF and annual daily precipitation (Pr) over 26 years
370 from simulations and reference datasets are displayed in Figure 9. And the statistical measure-
371 ments over whole CA area are showed in Table 4. As we can see, precipitation is distributed
372 mostly along the North coast and Sierra Nevada mountains, and is relatively sparse in other re-
373 gions. As temperature, simulations also captured the spatial patterns of the PRISM, with high
374 correlation coefficients (>0.94). However, there do exist clear differences among simulations.

375 Varres-CESM overestimated precipitation, especially in the coarser resolution (28 km) simu-
376 lation (about 40%-50%) along the western side of Sierra Nevada, resulting statistical difference
377 over this area comparing with PRISM. Interestingly, varres-CESM 0.125° is statistically the same
378 as PRISM. Uniform CESM has slightly better results than varres-CESM 0.25° deg. There are no-
379 table differences between WRF 27km and WRF 9km. WRF 27km underestimates precipitation
380 for about 30%, whereas WRF 9km shows a large positive difference (about 60%-80%) along the
381 North coast and the Sierra Nevada. However, considering the variability showed in the Figure
382 10, WRF 9km and WRF 27km are both significantly the same at the significance level of 0.05 as
383 PRISM except over the mountain region. From the sample standard deviation of the precipitation
384 displayed in Figure 10, we can see that the variability has similar patterns of the precipitation
385 intensity distribution, and increases as the precipitation magnitude increases. Models seem to
386 capture the variation of precipitation well, particularly looking at the varres-CESM 0.125° deg and
387 WRF 27 km, though variability is \sim 50% higher for WRF9km.

388 IThe reference datasets again showed differences indicating uncertainty inherent in interpolating
389 station data to a grid. We have also made the Student's t-test to test the if the mean precipitation
390 climatology from PRISM, UW and Daymet are statistically different from each other. And it
391 turned out that they are almost the same at the significance level of 0.05 over all the study area.
392 Therefore, the uncertainties within them are negligible. Overall, varres-CESM 0.125° performs
393 slightly better than CESM 0.25° and WRF 27km, as further exhibited by the RMSD values in
394 Table 4.

395 The annual cycle of precipitation averaged over each sub-zone over 26 years is presented in
396 Figure 11. It can be seen that simulations showed similar trend as reference datasets. The main
397 deviation occurred during the rainy seasons, especially in winter. WRF 27km is dryer and WRF
398 9km is far wetter in all regions as discussed above. Varres-CESM tracks well with observed pre-

399 cipitation everywhere except in the Central Valley, where precipitation is overestimated at rainy
400 seasons with about 70%-80%. Nonetheless, the strong seasonal dependence on precipitation is
401 apparent with extremely dry conditions during summer months. A slight increase in summertime
402 precipitation is apparent in the Desert region, indicating the North American monsoon. Over-
403 all, varres-CESM is more consistent with observations compared with WRF. However, we also
404 observe that the peak month for precipitation tends to occur earlier in varres-CESM than in obser-
405 vations. It is not surprising that a seasonal time drift occurred with the varres-CESM simulations
406 as it was not forced by a reanalysis dataset (unlike the WRF simulations).

407 The variability over each month is expressed by the sample standard deviation showed in Figure
408 12. The variability has similar monthly trend as the annual cycle of precipitation, with overall
409 value from 0 to 4 mm/day, which generally shows higher inter-annual variability over locations
410 of higher mean precipitation 11. Comparing with observations, varres-CESM exhibited a slightly
411 larger variability (basically no more than 1mm/day) in the rainy season, while WRF 27km has
412 better representation with a little lower values. WRF 9km again showed larger variability (about
413 ~1mm/day more) during rainy seasons over most regions. Such higher variability within higher
414 magnitude of precipitation has also been found in previous studies. Duffy et al. (2006) discussed
415 the higher variability caused by higher spatial resolution used in RCM models, with more accurate
416 representation of topography (Duffy et al. 2006). The main cause of the interannual variability of
417 precipitation over CA is El NioSouthern Oscillation (ENSO), which varies the amount of moisture
418 flux transported to this region.

419 The frequency distribution of DJF Pr has been constructed from rainy days in winter
420 ($Pr \geq 0.1 \text{ mm/d}$) and depicted in Figure 13. Within our expectation, it can be seen that varres-
421 CESM is more consistent with observations everywhere except in the CV. In this region WRF
422 27km appears to better capture high-intensity precipitation events, but performs more poorly on

423 low-intensity events. The underestimation of rainfall frequency in WRF 27km appears consis-
424 tent across regions. WRF 9km produces a significantly better treatment of low-intensity events,
425 but greatly overestimates the frequency of high-intensity events. Notably, varres-CESM 0.25 de-
426 gree and varres-CESM 0.125 degree do not show significant differences. For strong precipitation
427 events, varres-CESM and WRF 27km show good performance over most regions except in those
428 noted above, although these conclusions are also constrained by observational uncertainty.

429 The overestimation of precipitation for WRF at high resolution has also been found in previous
430 studies. Caldwell et al. (2009) showed that WRF at 12km largely overestimate the precipitation
431 over the mountain division of CA. The deviation magnitude is less than what showed in this study
432 due to different division area and perhaps different setting of physical schemes. In aforementioned
433 Caldwell's paper, possible reasons have been discussed in detail, stating a variety of source includ-
434 ing the model itself and the choice of physical parameterizations. A comprehensive analysis of the
435 cause of these errors is beyond the scope of this paper. Further discussion can be found in former
436 studies including the use of different microphysics schemes and resulting change of precipitation
437 magnitude (Leung et al. 2003b; Jankov et al. 2005; Gallus Jr and Bresch 2006; Chin et al. 2010;
438 Caldwell 2010).

439 Finally, a concise summary of model performance over CA is provided by the Taylor diagram
440 (Figure 14). This diagram includes the spatial centered correlation between the simulated and
441 observed fields, the RMS variability of simulations normalized by that in the observations, and
442 mean differences from reference data. It can be seen that the models correlate well with the PRISM
443 reference dataset. Normalized standard deviation and bias are larger for precipitation, especially
444 for WRF 9km. Overall, varres-CESM has demonstrated that it can competitively compare to WRF
445 in capturing the regional climatology of California. ([update the plot](#))

⁴⁴⁶ **4. Discussions and summary**

⁴⁴⁷ With the need of high resolution to better study regional climate and extreme events, this study
⁴⁴⁸ got deep into the use of a variable-resolution GCM (i.e. varres-CESM) as an alternative way in
⁴⁴⁹ dynamical regional climate modeling. The performance of varres-CESM has been investigated in
⁴⁵⁰ simulating California climatology as regional climate studies. This relatively new technique has
⁴⁵¹ been evaluated against a traditional RCM (i.e. WRF) directly for the first time.

⁴⁵² Based on 26 years of high-resolution historical climate simulations, we analyzed the mean cli-
⁴⁵³ matology of California and across its climate divisions from both temperature and precipitation,
⁴⁵⁴ mainly based on the output of varres-CESM and WRF. Generally, when compared with gridded
⁴⁵⁵ observational datasets, all simulations do a good job of capturing regional climatological patterns
⁴⁵⁶ with high spatial correlations (>0.94). Uncertainty between reference datasets exists, but is rela-
⁴⁵⁷ tively small and not statistically significant over most regions. We found that varres-CESM showed
⁴⁵⁸ comparable performance as WRF in regional climate study. Even compared with a uniform high-
⁴⁵⁹ resolution GCM (CESM-FV), varres-CESM also performed competitively.

⁴⁶⁰ Deviations from reference datasets do exist in these simulations, but they have different features.
⁴⁶¹ During summer, varres-CESM model possessed about 2 to 3°C warmer climate, especially in
⁴⁶² the Central Valley. WRF exhibited a colder ($\sim 2^{\circ}\text{C}$) Tmax over most regions except the Central
⁴⁶³ Valley, but a little warmer in Tmin. Overall, varres-CESM showed better ability in reproducing
⁴⁶⁴ mean climatology of Tmax, but WRF was better at modeling Tmin and Tavg. The variability of
⁴⁶⁵ JJA mean temperature is basically within the range of 0.5 to 1.5°C . WRF presents the annual
⁴⁶⁶ cycle of Tavg better than CESM with about 1°C underestimation. CESMs showed about 2°C
⁴⁶⁷ overestimation of Tavg over the summer season and similar magnitude of underestimation over
⁴⁶⁸ winter season, indicating larger temperature range over most regions.

⁴⁶⁹ For representation of heat extremes, both varres-CESM and WRF 27km exhibit close frequency
⁴⁷⁰ to observations over all study area except in Central Valley (CV). This is likely caused by the
⁴⁷¹ lack of irrigation cooling effect over this region since irrigation is rarely considered in long-term
⁴⁷² climate modeling. In future work, we will add irrigation effect in varres-CESM to figure out the
⁴⁷³ role irrigation played in regulating Tmax, and the overestimation and longer upbounded tail of
⁴⁷⁴ frequency distribution for Tmax,

⁴⁷⁵ As for precipitation representation, varres-CESM overestimates winter or annual precipitation
⁴⁷⁶ (about 40%-50%) especially along the western side of Sierra Nevada, and finer resolution simu-
⁴⁷⁷ lation produces a slight reduction (10%) likely due to improved treatment of orographic effects.
⁴⁷⁸ WRF 27km underestimates precipitation (about 30%) along the North coast and Sierra Nevada
⁴⁷⁹ mountains, where almost all the precipitation comes from, whereas WRF 9km shows a large
⁴⁸⁰ overestimation (about 70%–80%). Variability of precipitation ranges from 0 to 6 mm/day, with
⁴⁸¹ generally higher inter-annual variability over locations of higher mean precipitation. For strong
⁴⁸² precipitation events probability, varres-CESM and WRF 27km show satisfactory modeling ability
⁴⁸³ over most regions (except at the Central Valley for varres-CESM), although the reference datasets
⁴⁸⁴ also show some uncertainties.

⁴⁸⁵ Higher resolution (0.125°) simulation of varres-CESM do show better results in capturing sum-
⁴⁸⁶ mer Tmax, precipitation and their variablility, than the coarser resolution run. However, the im-
⁴⁸⁷ provements are not statistically significant. For WRF, when resolution increased, the model pro-
⁴⁸⁸ duces obviously overestimated precipitation as previous studies have also found when using RCMs
⁴⁸⁹ for fine-scale simulations as aforementioned. The use convection scheme is perhaps not needed
⁴⁹⁰ when grid spacing is near 10km. However, it turned out that almost all of the precipitation comes
⁴⁹¹ from resolved (large-scale) processes for all these models. In this way, model deviation is mainly

492 related with resolved-scale processes and microphysics scheme plays a major role, which makes
493 it necessary to develop more scale-aware parameterizations.

494 The importance and necessity of high resolution for regional climate studies has been widely
495 stressed by previous studies. However, whether the current regional climate models can fulfill this
496 demand when resolution is pushed to local scales is questionable. It is clear that further work is
497 urgently needed to solve the scale limitation of current regional climate models at fine horizontal
498 resolutions. The possible causes of the scale limitation may include a lack of accurate scale-aware
499 physical parameterizations near or below 10 km horizontal resolution, the treatment of dynamics
500 at fine scales, and the interactions among different components of RCMs or VR-GCMs (e.g., land-
501 atmosphere interactions).

502 In summary, varres-CESM demonstrated competitive utility for studying high-resolution re-
503 gional climatology when compared to a regional climate model (WRF) and a uniform high-
504 resolution GCM (CESM-FV). Deviations, showed within these models, are not indicative of deep
505 underlying problems with the model formulation, but one should be aware of these differences
506 when using these models for assessing future climate change. This study suggests that variable-
507 resolution GCMs are useful tools for assessing climate change over the coming century. As the
508 need for assessments of regional climate change is increasing, alternative modeling strategies, in-
509 cluding variable-resolution global climate models will be needed to improve our understanding of
510 the effects of fine-scale processes representation in regional climate regulation.

511 *Acknowledgments.* The authors would like to thank Michael Wehner and Daíthí Stone for pro-
512 viding the uniform resolution CESM dataset. We would further like to thank Travis O'Brien for
513 his many useful conversations on climate model assessment. We also want to thank Xuemeng
514 Chen for her assistance in WRF running. This project is supported in part by the University of

515 California, Davis and by the Department of Energy “Multiscale Methods for Accurate, Efficient,
516 and Scale-Aware Models of the Earth System” program.

517 **References**

- 518 Abatzoglou, J. T., K. T. Redmond, and L. M. Edwards, 2009: Classification of regional climate
519 variability in the state of California. *Journal of Applied Meteorology and Climatology*, **48** (8),
520 1527–1541.
- 521 Bacmeister, J. T., M. F. Wehner, R. B. Neale, A. Gettelman, C. Hannay, P. H. Lauritzen, J. M.
522 Caron, and J. E. Truesdale, 2014: Exploratory high-resolution climate simulations using the
523 Community Atmosphere Model (CAM). *Journal of Climate*, **27** (9), 3073–3099.
- 524 Bonfils, C., and D. Lobell, 2007: Empirical evidence for a recent slowdown in irrigation-induced
525 cooling. *Proceedings of the National Academy of Sciences*, **104** (34), 13 582–13 587.
- 526 Bukovsky, M. S., and D. J. Karoly, 2007: A brief evaluation of precipitation from the North
527 American Regional Reanalysis. *Journal of Hydrometeorology*, **8** (4), 837–846.
- 528 Bukovsky, M. S., and D. J. Karoly, 2009: Precipitation simulations using WRF as a nested regional
529 climate model. *Journal of Applied Meteorology and Climatology*, **48** (10), 2152–2159.
- 530 Caldwell, P., 2010: California wintertime precipitation bias in regional and global climate models.
531 *Journal of Applied Meteorology and Climatology*, **49** (10), 2147–2158.
- 532 Caldwell, P., H.-N. S. Chin, D. C. Bader, and G. Bala, 2009: Evaluation of a WRF dynamical
533 downscaling simulation over California. *Climatic Change*, **95** (3-4), 499–521.
- 534 Cayan, D. R., A. L. Luers, G. Franco, M. Hanemann, B. Croes, and E. Vine, 2008: Overview of
535 the California climate change scenarios project. *Climatic Change*, **87** (1), 1–6.

- 536 Chen, F., and J. Dudhia, 2001: Coupling an advanced land surface-hydrology model with the Penn
537 State-NCAR MM5 modeling system. Part I: Model implementation and sensitivity. *Monthly*
538 *Weather Review*, **129** (4), 569–585.
- 539 Chin, H.-N. S., P. M. Caldwell, and D. C. Bader, 2010: Preliminary study of California wintertime
540 model wet bias. *Monthly Weather Review*, **138** (9), 3556–3571.
- 541 Christensen, J. H., and Coauthors, 2007: Regional climate projections. *Climate Change, 2007:*
542 *The Physical Science Basis. Contribution of Working group I to the Fourth Assessment Report*
543 *of the Intergovernmental Panel on Climate Change, University Press, Cambridge, Chapter 11,*
544 847–940.
- 545 Collins, W. D., and Coauthors, 2004: Description of the NCAR community atmosphere model
546 (CAM 3.0). Tech. rep., Tech. Rep. NCAR/TN-464+ STR.
- 547 Daly, C., M. Halbleib, J. I. Smith, W. P. Gibson, M. K. Doggett, G. H. Taylor, J. Curtis, and P. P.
548 Pasteris, 2008: Physiographically sensitive mapping of climatological temperature and precip-
549 itation across the conterminous United States. *International Journal of Climatology*, **28** (15),
550 2031–2064.
- 551 Dee, D., and Coauthors, 2011: The ERA-Interim reanalysis: Configuration and performance of
552 the data assimilation system. *Quarterly Journal of the Royal Meteorological Society*, **137** (656),
553 553–597.
- 554 Dinse, K., 2009: Climate variability and climate change: what is the difference. *Book Climate*
555 *Variability and Climate Change: What is the Difference.*
- 556 Duffy, P., and Coauthors, 2006: Simulations of present and future climates in the western United
557 States with four nested regional climate models. *Journal of Climate*, **19** (6), 873–895.

- 558 Fox-Rabinovitz, M., J. Côté, B. Dugas, M. Déqué, and J. L. McGregor, 2006: Variable resolution
559 general circulation models: Stretched-grid model intercomparison project (SGMIP). *Journal of*
560 *Geophysical Research: Atmospheres (1984–2012)*, **111** (D16).
- 561 Fox-Rabinovitz, M. S., G. L. Stenchikov, M. J. Suarez, and L. L. Takacs, 1997: A finite-
562 difference GCM dynamical core with a variable-resolution stretched grid. *Monthly Weather*
563 *Review*, **125** (11), 2943–2968.
- 564 Fox-Rabinovitz, M. S., G. L. Stenchikov, M. J. Suarez, L. L. Takacs, and R. C. Govindaraju, 2000:
565 A uniform-and variable-resolution stretched-grid GCM dynamical core with realistic orography.
566 *Monthly Weather Review*, **128** (6), 1883–1898.
- 567 Fox-Rabinovitz, M. S., L. L. Takacs, R. C. Govindaraju, and M. J. Suarez, 2001: A variable-
568 resolution stretched-grid general circulation model: Regional climate simulation. *Monthly*
569 *Weather Review*, **129** (3), 453–469.
- 570 Gallus Jr, W. A., and J. F. Bresch, 2006: Comparison of impacts of WRF dynamic core, physics
571 package, and initial conditions on warm season rainfall forecasts. *Monthly Weather Review*,
572 **134** (9), 2632–2641.
- 573 Gates, W. L., 1992: AMIP: The Atmospheric Model Intercomparison Project. *Bulletin of the*
574 *American Meteorological Society*, **73**, 1962–1970.
- 575 Hamlet, A. F., and D. P. Lettenmaier, 2005: Production of Temporally Consistent Gridded Precipi-
576 tation and Temperature Fields for the Continental United States*. *Journal of Hydrometeorology*,
577 **6** (3), 330–336.

- 578 Hayhoe, K., and Coauthors, 2004: Emissions pathways, climate change, and impacts on California
579 *Proceedings of the National Academy of Sciences of the United States of America*, **101** (34),
580 12 422–12 427.
- 581 Hong, S.-Y., and J.-O. J. Lim, 2006: The WRF single-moment 6-class microphysics scheme
582 (*WSM6*). *Asia-Pacific Journal of Atmospheric Sciences*, **42** (2), 129–151.
- 583 Hong, S.-Y., Y. Noh, and J. Dudhia, 2006: A new vertical diffusion package with an explicit
584 treatment of entrainment processes. *Monthly Weather Review*, **134** (9), 2318–2341.
- 585 Hurrell, J. W., J. J. Hack, D. Shea, J. M. Caron, and J. Rosinski, 2008: A new sea surface temper-
586 ature and sea ice boundary dataset for the Community Atmosphere Model. *Journal of Climate*,
587 **21** (19), 5145–5153.
- 588 Hurrell, J. W., and Coauthors, 2013: The community earth system model: A framework for col-
589 laborative research. *Bulletin of the American Meteorological Society*, **94** (9), 1339–1360.
- 590 Jankov, I., W. A. Gallus Jr, M. Segal, B. Shaw, and S. E. Koch, 2005: The impact of different WRF
591 model physical parameterizations and their interactions on warm season MCS rainfall. *Weather*
592 and Forecasting, **20** (6), 1048–1060.
- 593 Kain, J. S., 2004: The Kain-Fritsch convective parameterization: An update. *Journal of Applied*
594 *Meteorology*, **43** (1), 170–181.
- 595 Kanamitsu, M., and H. Kanamaru, 2007: Fifty-seven-year California Reanalysis Downscaling at
596 10 km (CaRD10). Part I: System detail and validation with observations. *Journal of Climate*,
597 **20** (22), 5553–5571.
- 598 Kueppers, L. M., M. A. Snyder, and L. C. Sloan, 2007: Irrigation cooling effect: Regional climate
599 forcing by land-use change. *Geophysical Research Letters*, **34** (3).

- 600 Laprise, R., 2008: Regional climate modelling. *Journal of Computational Physics*, **227** (7), 3641–
601 3666.
- 602 Laprise, R., and Coauthors, 2008: Challenging some tenets of regional climate modelling. *Meteo-*
603 *rology and Atmospheric Physics*, **100** (1-4), 3–22.
- 604 Leung, L. R., L. O. Mearns, F. Giorgi, and R. L. Wilby, 2003a: Regional climate research: needs
605 and opportunities. *Bulletin of the American Meteorological Society*, **84** (1), 89–95.
- 606 Leung, L. R., and Y. Qian, 2009: Atmospheric rivers induced heavy precipitation and flooding in
607 the western US simulated by the WRF regional climate model. *Geophysical research letters*,
608 **36** (3).
- 609 Leung, L. R., Y. Qian, and X. Bian, 2003b: Hydroclimate of the western United States based on
610 observations and regional climate simulation of 1981-2000. Part I: Seasonal statistics. *Journal*
611 *of Climate*, **16** (12), 1892–1911.
- 612 Leung, L. R., Y. Qian, X. Bian, W. M. Washington, J. Han, and J. O. Roads, 2004: Mid-century
613 ensemble regional climate change scenarios for the western United States. *Climatic Change*,
614 **62** (1-3), 75–113.
- 615 Lo, J. C.-F., Z.-L. Yang, and R. A. Pielke, 2008: Assessment of three dynamical climate downscal-
616 ing methods using the Weather Research and Forecasting (WRF) model. *Journal of Geophysical*
617 *Research: Atmospheres (1984–2012)*, **113** (D9).
- 618 Maurer, E., A. Wood, J. Adam, D. Lettenmaier, and B. Nijssen, 2002: A long-term hydrologically
619 based dataset of land surface fluxes and states for the conterminous United States*. *Journal of*
620 *climate*, **15** (22), 3237–3251.

- 621 McDonald, A., 2003: Transparent boundary conditions for the shallow-water equations: testing in
622 a nested environment. *Monthly Weather Review*, **131** (4), 698–705.
- 623 Mearns, L. O., and Coauthors, 2012: The North American regional climate change assessment
624 program: overview of phase I results. *Bulletin of the American Meteorological Society*, **93** (9),
625 1337–1362.
- 626 Mesinger, F., and K. Veljovic, 2013: Limited area NWP and regional climate modeling: a test
627 of the relaxation vs Eta lateral boundary conditions. *Meteorology and Atmospheric Physics*,
628 **119** (1-2), 1–16.
- 629 Mesinger, F., and Coauthors, 2006: North American regional reanalysis. *Bulletin of the American*
630 *Meteorological Society*, **87**, 343–360.
- 631 Neale, R. B., and Coauthors, 2010a: Description of the NCAR community atmosphere model
632 (CAM 5.0). *NCAR Tech. Note NCAR/TN-486+STR*.
- 633 Neale, R. B., and Coauthors, 2010b: Description of the NCAR Community Atmosphere Model
634 (CAM 5.0). NCAR Technical Note NCAR/TN-486+STR, National Center for Atmospheric Re-
635 search, Boulder, Colorado, 268 pp.
- 636 Oleson, K., and Coauthors, 2010: Technical description of version 4.0 of the Community Land
637 Model (CLM). NCAR Technical Note NCAR/TN-478+STR, National Center for Atmospheric
638 Research, Boulder, Colorado, 257 pp. doi:10.5065/D6FB50WZ.
- 639 Pan, L.-L., S.-H. Chen, D. Cayan, M.-Y. Lin, Q. Hart, M.-H. Zhang, Y. Liu, and J. Wang, 2011:
640 Influences of climate change on California and Nevada regions revealed by a high-resolution
641 dynamical downscaling study. *Climate Dynamics*, **37** (9-10), 2005–2020.

- 642 Pierce, D. W., and Coauthors, 2013: Probabilistic estimates of future changes in California temper-
643 ature and precipitation using statistical and dynamical downscaling. *Climate Dynamics*, **40** (3-
644 4), 839–856.
- 645 Rauscher, S. A., E. Coppola, C. Piani, and F. Giorgi, 2010: Resolution effects on regional climate
646 model simulations of seasonal precipitation over Europe. *Climate Dynamics*, **35** (4), 685–711.
- 647 Rauscher, S. A., T. D. Ringler, W. C. Skamarock, and A. A. Mirin, 2013: Exploring a Global
648 Multiresolution Modeling Approach Using Aquaplanet Simulations. *Journal of Climate*, **26** (8),
649 2432–2452.
- 650 Ringler, T., L. Ju, and M. Gunzburger, 2008: A multiresolution method for climate system model-
651 ing: application of spherical centroidal voronoi tessellations. *Ocean Dynamics*, **58** (5-6), 475–
652 498.
- 653 Rummukainen, M., 2010: State-of-the-art with Regional Climate Models. *Wiley Interdisciplinary
654 Reviews: Climate Change*, **1** (1), 82–96.
- 655 Skamarock, W., J. Klemp, J. Dudhia, D. Gill, and D. Barker, 2005: Coauthors, 2008: A Descrip-
656 tion of the Advanced Research WRF Version 3. NCAR Technical Note. Tech. rep., NCAR/TN–
657 475+ STR.
- 658 Skamarock, W. C., and J. B. Klemp, 2008: A time-split nonhydrostatic atmospheric model for
659 weather research and forecasting applications. *Journal of Computational Physics*, **227** (7),
660 3465–3485.
- 661 Skamarock, W. C., J. B. Klemp, M. G. Duda, L. D. Fowler, S.-H. Park, and T. D. Ringler, 2012: A
662 multiscale nonhydrostatic atmospheric model using centroidal voronoi tesselations and c-grid
663 staggering. *Monthly Weather Review*, **140** (9), 3090–3105.

- 664 Soares, P. M., R. M. Cardoso, P. M. Miranda, J. de Medeiros, M. Belo-Pereira, and F. Espírito-
665 Santo, 2012: WRF high resolution dynamical downscaling of ERA-Interim for Portugal. *Cli-*
666 *mate dynamics*, **39 (9-10)**, 2497–2522.
- 667 Solomon, S., 2007: *Climate change 2007—the physical science basis: Working group I contribution*
668 *to the fourth assessment report of the IPCC*, Vol. 4. Cambridge University Press.
- 669 Staniforth, A. N., and H. L. Mitchell, 1978: A variable-resolution finite-element technique for
670 regional forecasting with the primitive equations. *Monthly Weather Review*, **106 (4)**, 439–447.
- 671 Stauffer, D. R., and N. L. Seaman, 1990: Use of four-dimensional data assimilation in a limited-
672 area mesoscale model. Part I: Experiments with synoptic-scale data. *Monthly Weather Review*,
673 **118 (6)**, 1250–1277.
- 674 Taylor, M. A., and A. Fournier, 2010: A compatible and conservative spectral element method on
675 unstructured grids. *Journal of Computational Physics*, **229 (17)**, 5879–5895.
- 676 Thornton, P. E., H. Hasenauer, and M. A. White, 2000: Simultaneous estimation of daily solar ra-
677 diation and humidity from observed temperature and precipitation: an application over complex
678 terrain in Austria. *Agricultural and Forest Meteorology*, **104 (4)**, 255–271.
- 679 Thornton, P. E., and S. W. Running, 1999: An improved algorithm for estimating incident daily
680 solar radiation from measurements of temperature, humidity, and precipitation. *Agricultural and*
681 *Forest Meteorology*, **93 (4)**, 211–228.
- 682 Thornton, P. E., S. W. Running, and M. A. White, 1997: Generating surfaces of daily meteorolog-
683 ical variables over large regions of complex terrain. *Journal of Hydrology*, **190 (3)**, 214–251.
- 684 Ullrich, P. A., 2014: SQuadGen: Spherical Quadrilateral Grid Generator. Accessed: 2015-02-11,
685 <http://climate.ucdavis.edu/squadgen.php>.

- 686 Warner, T. T., R. A. Peterson, and R. E. Treadon, 1997: A tutorial on lateral boundary conditions
687 as a basic and potentially serious limitation to regional numerical weather prediction. *Bulletin*
688 *of the American Meteorological Society*, **78** (11), 2599–2617.
- 689 Wehner, M., Prabhat, K. Reed, D. Stone, W. D. Collins, J. Bacmeister, and A. Gettleman, 2014a:
690 Resolution dependence of future tropical cyclone projections of CAM5.1 in the US CLIVAR
691 Hurricane Working Group idealized configurations. *J. Climate*, doi:10.1175/JCLI-D-14-00311.
692 1, in press.
- 693 Wehner, M. F., and Coauthors, 2014b: The effect of horizontal resolution on simulation qual-
694 ity in the Community Atmospheric Model, CAM5.1. *J. Model. Earth. Sys.*, doi:10.1002/
695 2013MS000276.
- 696 Zarzycki, C. M., and C. Jablonowski, 2014: A multidecadal simulation of Atlantic tropical cy-
697 clones using a variable-resolution global atmospheric general circulation model. *Journal of Ad-*
698 *vances in Modeling Earth Systems*, **6** (3), 805–828.
- 699 Zarzycki, C. M., C. Jablonowski, and M. A. Taylor, 2014: Using Variable-Resolution Meshes
700 to Model Tropical Cyclones in the Community Atmosphere Model. *Monthly Weather Review*,
701 **142** (3), 1221–1239.
- 702 Zarzycki, C. M., C. Jablonowski, D. R. Thatcher, and M. A. Taylor, 2015: Effects of localized
703 grid refinement on the general circulation and climatology in the community atmosphere model.
704 *Journal of Climate*, **28** (7), 2777–2803.

705 **LIST OF TABLES**

706 Table 1.	Reanalysis and statistically downscaled observational datasets used in this	34
707 study.		
708 Table 2.	RMSD, MAD and Correlation (Corr) for JJA temperature over California	35
709 Table 3.	The first four moments of the JJA Tmax frequency in each sub-zone. Column	
710 titles refer to Average (Avg), Variance (Var), Skewness (Skew) and Kurtosis		
711 (Kurt).		36
712 Table 4.	RMSD, MAD, MRD, Correlation (Corr) for precipitation over California	37

TABLE 1. Reanalysis and statistically downscaled observational datasets used in this study.

Data source	Variables used	Spatial resolution	Temporal resolution
NARR	Pr, T_s	32km	daily, 3-hourly
NCEP CPC	Pr	0.125°	daily
UW	Pr, T_{min} , T_{max}	0.125°	daily
PRISM	Pr, T_{min} , T_{max} , T_{avg}	4km	monthly
Daymet	Pr, T_{min} , T_{max}	1km	daily

TABLE 2. RMSD, MAD and Correlation (Corr) for JJA temperature over California

RMSD	UW		PRISM			Daymet	
	T_{max}	T_{min}	T_{max}	T_{min}	T_{avg}	T_{max}	T_{min}
varres-CESM 0.25d	2.322	3.745	2.924	3.121	2.604	2.810	3.934
varres-CESM 0.125d	1.900	3.631	2.447	2.944	2.184	2.475	3.701
WRF 27km	2.310	2.738	2.933	2.254	2.169	2.511	2.992
WRF 9km	3.319	2.937	3.492	1.837	1.769	3.203	2.942
uniform CESM 0.25d	3.885	4.088	4.265	3.614	3.536	4.315	4.274
MAD	UW		PRISM			Daymet	
	T_{max}	T_{min}	T_{max}	T_{min}	T_{avg}	T_{max}	T_{min}
varres-CESM 0.25d	0.981	2.907	0.606	1.731	0.823	1.177	2.877
varres-CESM 0.125d	0.645	2.848	0.203	1.660	0.579	0.818	2.744
WRF 27km	-0.577	0.819	-0.952	-0.357	-0.771	-0.386	0.789
WRF 9km	-2.277	1.862	-2.720	0.674	-1.142	-2.103	1.757
uniform CESM 0.25d	1.812	2.993	1.449	1.815	1.280	2.013	2.961
Corr	UW		PRISM			Daymet	
	T_{max}	T_{min}	T_{max}	T_{min}	T_{avg}	T_{max}	T_{min}
varres-CESM 0.25d	0.998	0.982	0.996	0.986	0.994	0.997	0.979
varres-CESM 0.125d	0.998	0.985	0.997	0.988	0.996	0.997	0.983
WRF 27km	0.997	0.982	0.996	0.989	0.996	0.997	0.978
WRF 9km	0.996	0.985	0.997	0.993	0.998	0.996	0.984
uniform CESM 0.25d	0.994	0.980	0.992	0.981	0.991	0.993	0.977

713 TABLE 3. The first four moments of the JJA Tmax frequency in each sub-zone. Column titles refer to Average
 714 (Avg), Variance (Var), Skewness (Skew) and Kurtosis (Kurt).

	Central valley				Mountain				North coast				South coast				Desert			
	Avg	Var	Skew	Kurt	Avg	Var	Skew	Kurt	Avg	Var	Skew	Kurt	Avg	Var	Skew	Kurt	Avg	Var	Skew	Kurt
UW	32.6	24.8	-0.8	0.9	26.7	33.2	-0.4	0.3	25.9	30.4	0.1	-0.5	25.9	30.4	0.1	-0.5	37.0	22.9	-0.6	0.7
Daymet	32.7	23.5	-0.9	1.5	25.9	39.3	-0.5	0.5	26.5	30.1	-0.3	0.4	26.5	30.1	-0.3	0.4	37.0	24.3	-0.6	0.6
CESM 0.25d	34.1	26.2	-0.4	0.2	28.1	27.6	-0.4	0.3	26.4	37.4	0.1	-0.7	26.4	37.4	0.1	-0.7	37.6	19.0	-0.5	0.8
CESM 0.125d	34.3	28.5	-0.5	0.4	27.2	30.0	-0.4	0.3	26.3	37.4	0.1	-0.6	26.3	37.4	0.1	-0.6	37.3	21.3	-0.5	0.4
WRF 27km	33.9	34.8	-0.5	0.2	24.9	34.8	-0.3	0.0	26.0	36.7	-0.1	-0.5	26.0	36.7	-0.1	-0.5	36.5	22.6	-0.6	0.5
WRF 9km	32.4	33.1	-0.7	0.6	22.4	38.5	-0.5	0.6	24.9	32.6	0.0	-0.6	24.9	32.6	0.0	-0.6	34.4	24.4	-0.5	0.4

Notes: If skew > 0 [skew < 0], the distribution trails off to the right [left]. If kurtosis > 0 [< 0], it is usually more sharply peaked [flatter] than the normal distribution (leptokurtic and platykurtic, respectively).

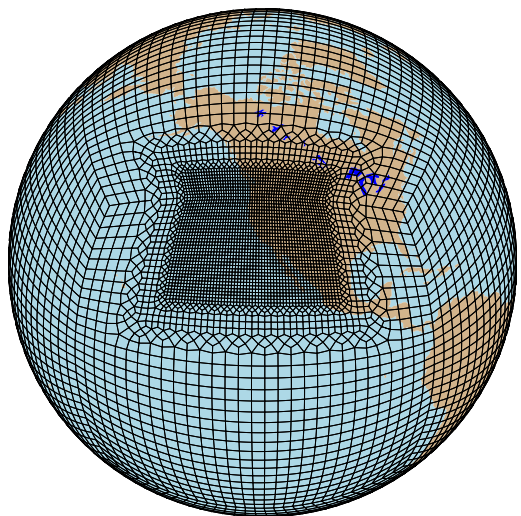
TABLE 4. RMSD, MAD, MRD, Correlation (Corr) for precipitation over California

Annual	CPC				UW				PRISM				DAYMET				
	RMSD	MAD	MRD	Corr	RMSD	MAD	MRD	Corr	RMSD	MAD	MRD	Corr	RMSD	MAD	MRD	Corr	
varres-CESM 0.25d	0.607	0.394	0.413	0.981	0.616	0.292	0.434	0.968	0.727	0.203	0.429	0.952	0.567	0.191	0.375	0.972	
varres-CESM 0.125d	0.469	0.207	0.321	0.980	0.526	0.115	0.339	0.970	0.624	0.045	0.328	0.961	0.504	0.027	0.310	0.973	
WRF 27km	0.419	-0.205	0.269	0.977	0.580	-0.308	0.274	0.971	0.765	-0.396	0.296	0.965	0.647	-0.409	0.312	0.970	
WRF 9km	2.226	1.485	0.950	0.957	2.052	1.393	0.864	0.964	1.889	1.322	0.815	0.970	2.005	1.306	0.773	0.961	
uniform CESM 0.25d	0.555	0.134	0.277	0.969	0.600	0.031	0.302	0.961	0.700	-0.057	0.290	0.953	0.600	-0.069	0.284	0.962	
DJF		CPC				UW				PRISM				DAYMET			
		RMSD	MAD	MRD	Corr	RMSD	MAD	MRD	Corr	RMSD	MAD	MRD	Corr	RMSD	MAD	MRD	Corr
varres-CESM 0.25d	1.486	0.986	0.532	0.972	1.445	0.673	0.531	0.959	1.654	0.577	0.547	0.943	1.346	0.514	0.435	0.964	
varres-CESM 0.125d	1.194	0.638	0.396	0.976	1.234	0.346	0.398	0.965	1.395	0.287	0.400	0.955	1.170	0.212	0.337	0.969	
WRF 27km	0.888	-0.376	0.269	0.975	1.289	-0.688	0.289	0.967	1.552	-0.785	0.298	0.962	1.351	-0.848	0.324	0.966	
WRF 9km	4.264	2.607	0.742	0.950	3.835	2.315	0.616	0.955	3.570	2.256	0.604	0.964	3.804	2.183	0.554	0.955	
uniform CESM 0.25d	1.392	0.377	0.300	0.960	1.431	0.064	0.316	0.951	1.544	-0.033	0.314	0.946	1.406	-0.095	0.288	0.953	

715 LIST OF FIGURES

716	Fig. 1. Grid meshes for the two varres-CESM simulations.	39
717	Fig. 2. Domains of WRF simulations (left) and five climate divisions in California (right) with	
718	topography in meters (m).	40
719	Fig. 3. Topography in meters (m) for (top left to bottom right) varres-CESM 0.25° , varres-CESM	
720	0.125° , uniform CESM-FV 0.25° , WRF 27km, WRF 9km and ERA-Interim (~ 80 km).	41
721	Fig. 4. JJA average daily Tmax, Tmin and Tavg from models and reference datasets, and differences	
722	between them ($^\circ\text{C}$).	42
723	Fig. 5. sample standard deviation of JJA average daily Tmax, Tmin and Tavg from models and	
724	PRISM ($^\circ\text{C}$).	43
725	Fig. 6. Seasonal cycle of monthly-average Tavg for each subzone ($^\circ\text{C}$). Bars represent standard	
726	deviation (σ) values.	44
727	Fig. 7. Seasonal standard deviation (s) values of monthly-average Tavg for each subzone ($^\circ\text{C}$). Bars	
728	represent standard deviation (s) values.	45
729	Fig. 8. Frequency distribution of summer Tmax ($^\circ\text{C}$).	46
730	Fig. 9. Annual and DJF precipitation from models and reference datasets (mm/d).	47
731	Fig. 10. sample standard deviation of Annual and DJF precipitation from models and PRISM	
732	(mm/d).	48
733	Fig. 11. As Figure 6, but for monthly-average total precipitation (mm/d).	49
734	Fig. 12. As Figure 7, but for monthly-average total precipitation (mm/d).	50
735	Fig. 13. Frequency distribution of winter Pr constructed from 26 years of daily data (mm/d) (note	
736	that the vertical scale is logarithmic).	51
737	Fig. 14. Taylor diagram of annual climatology for the entire California region, using the PRISM	
738	dataset as reference.	52

1 degree -> 0.25 degree



1 degree -> 0.125 degree

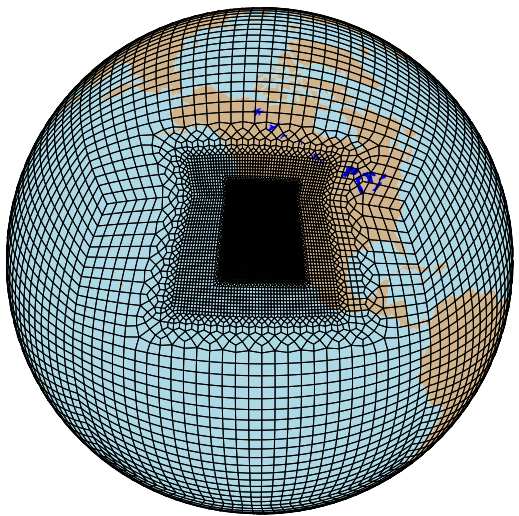
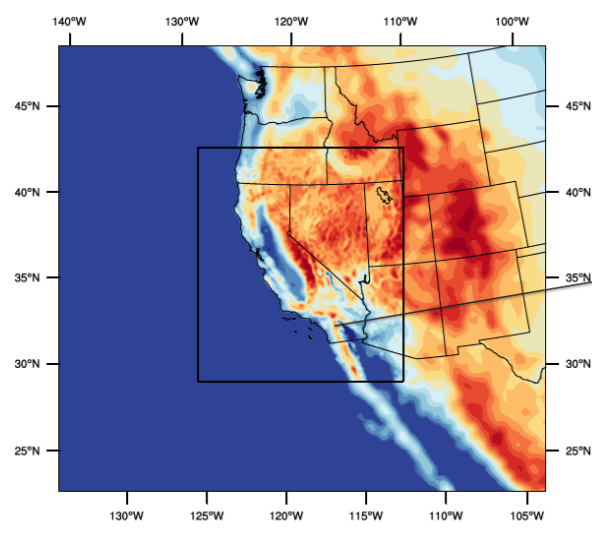
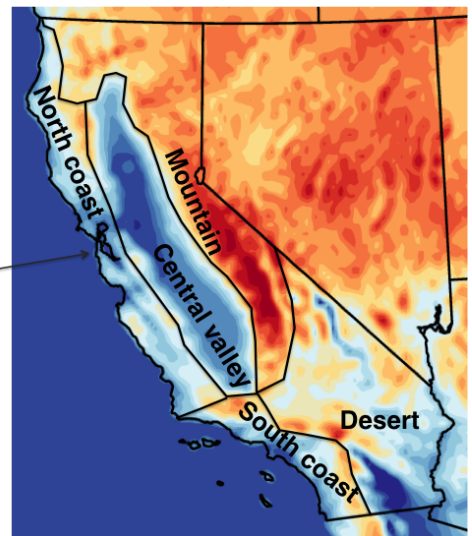


FIG. 1. Grid meshes for the two varres-CESM simulations.

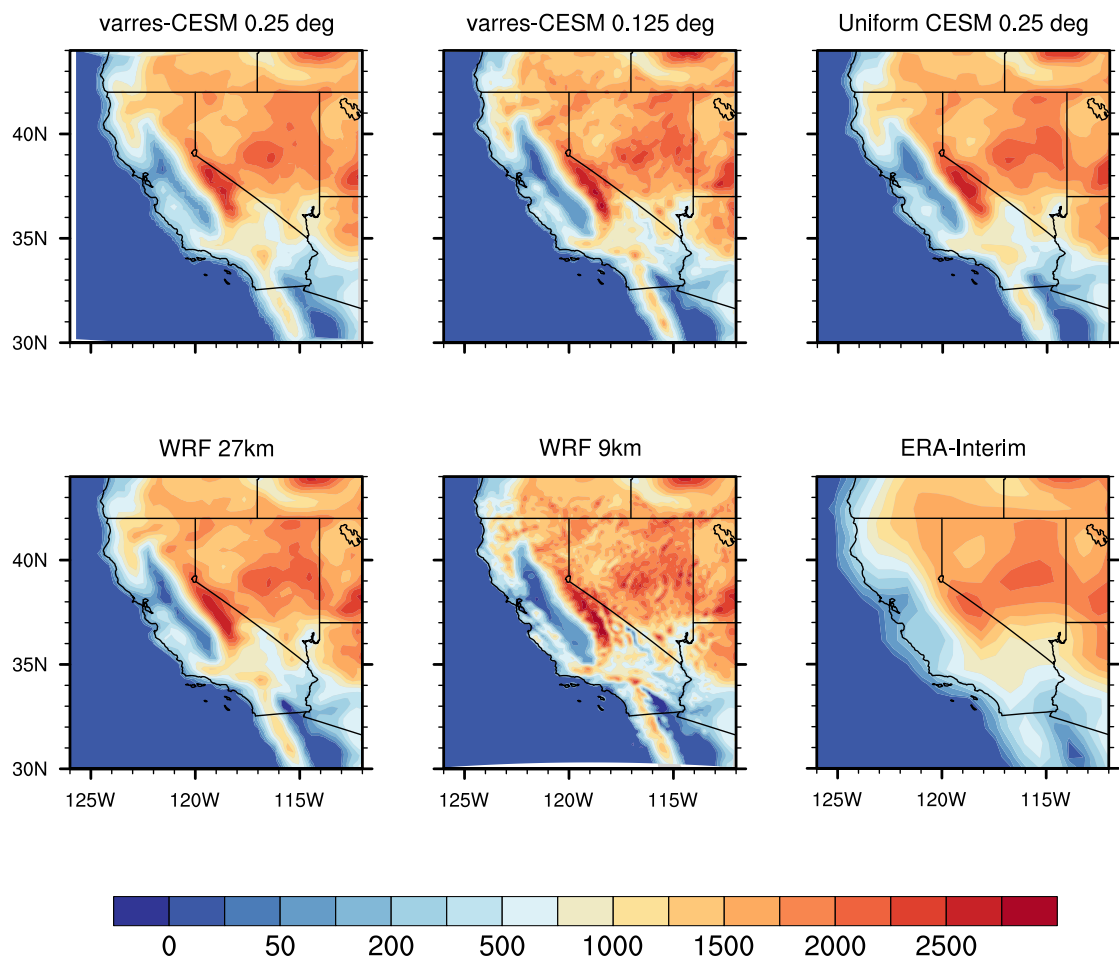
WRF 9km : Outer and inner domain



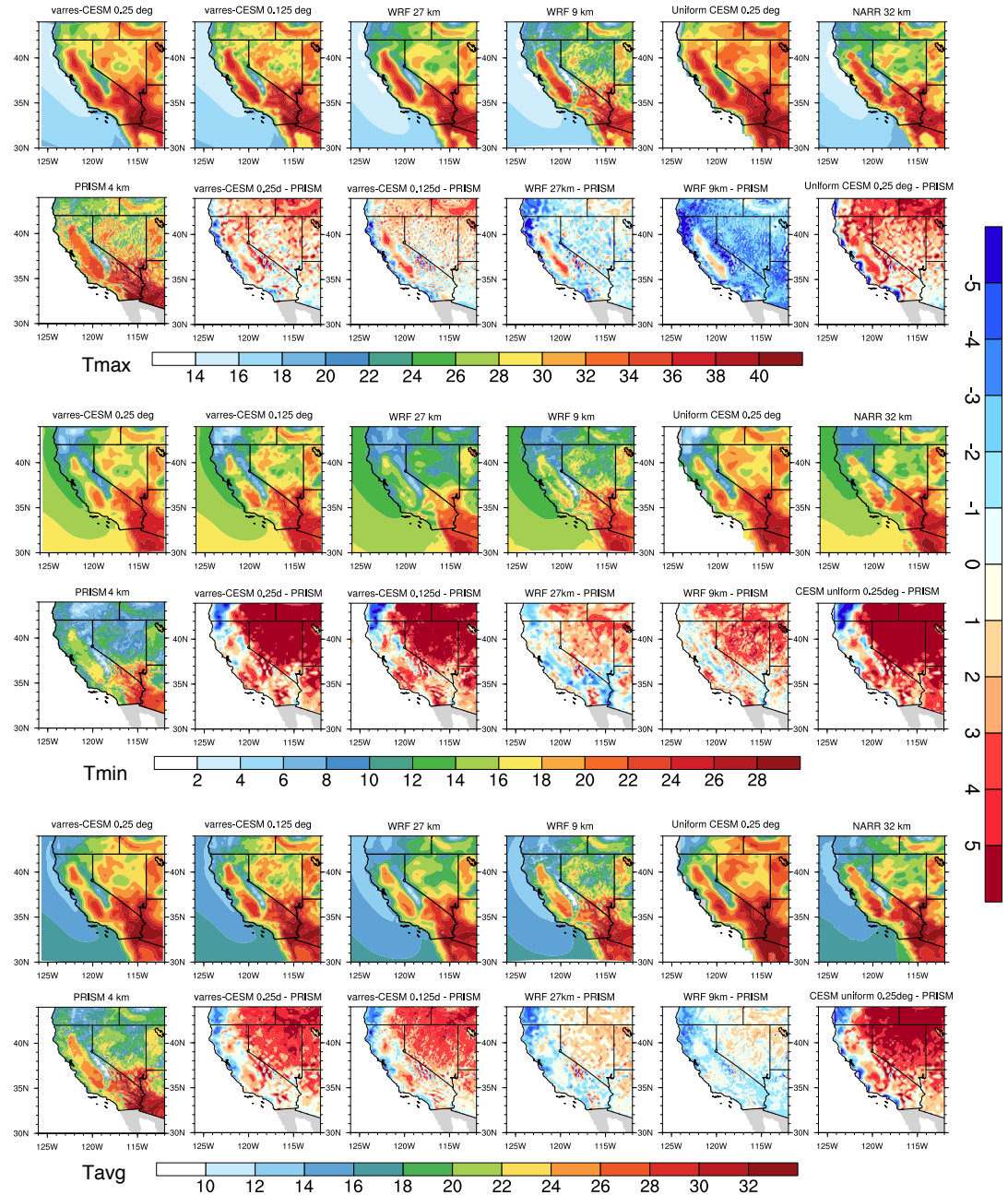
Climate divisions across CA



739 FIG. 2. Domains of WRF simulations (left) and five climate divisions in California (right) with topography in
740 meters (m).



741 FIG. 3. Topography in meters (m) for (top left to bottom right) varres-CESM 0.25° , varres-CESM 0.125° ,
 742 uniform CESM-FV 0.25° , WRF 27km, WRF 9km and ERA-Interim (~ 80 km).



743

FIG. 4. JJA average daily Tmax, Tmin and Tavg from models and reference datasets, and differences between them ($^{\circ}\text{C}$).

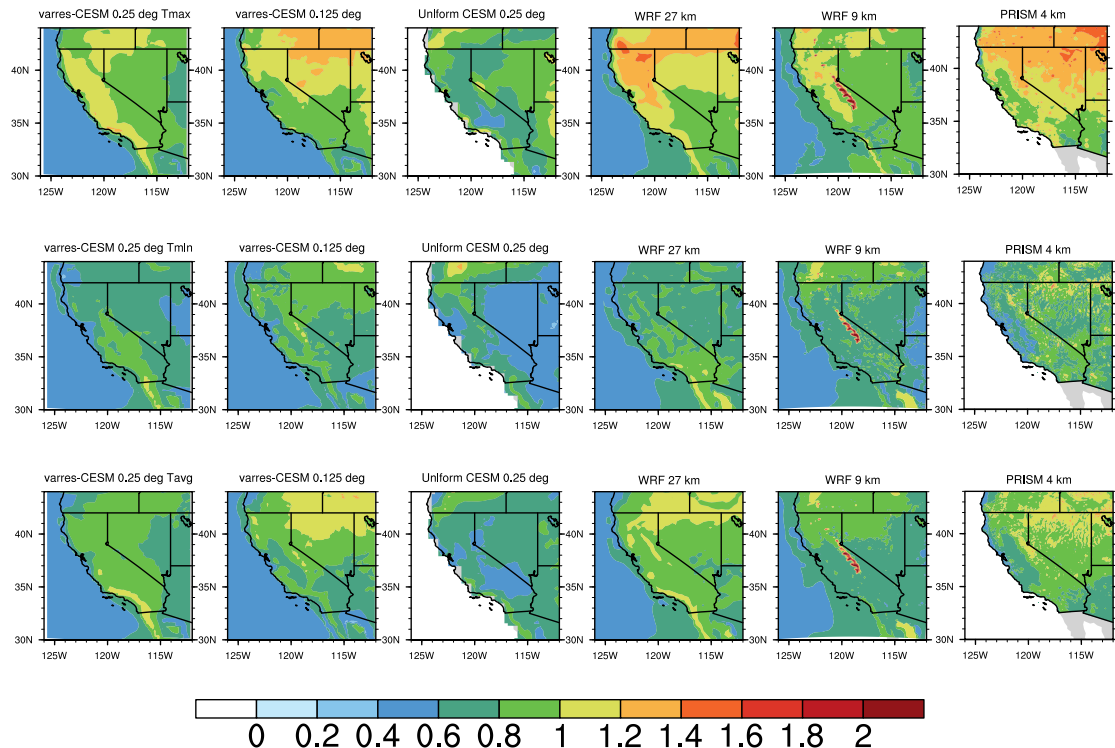
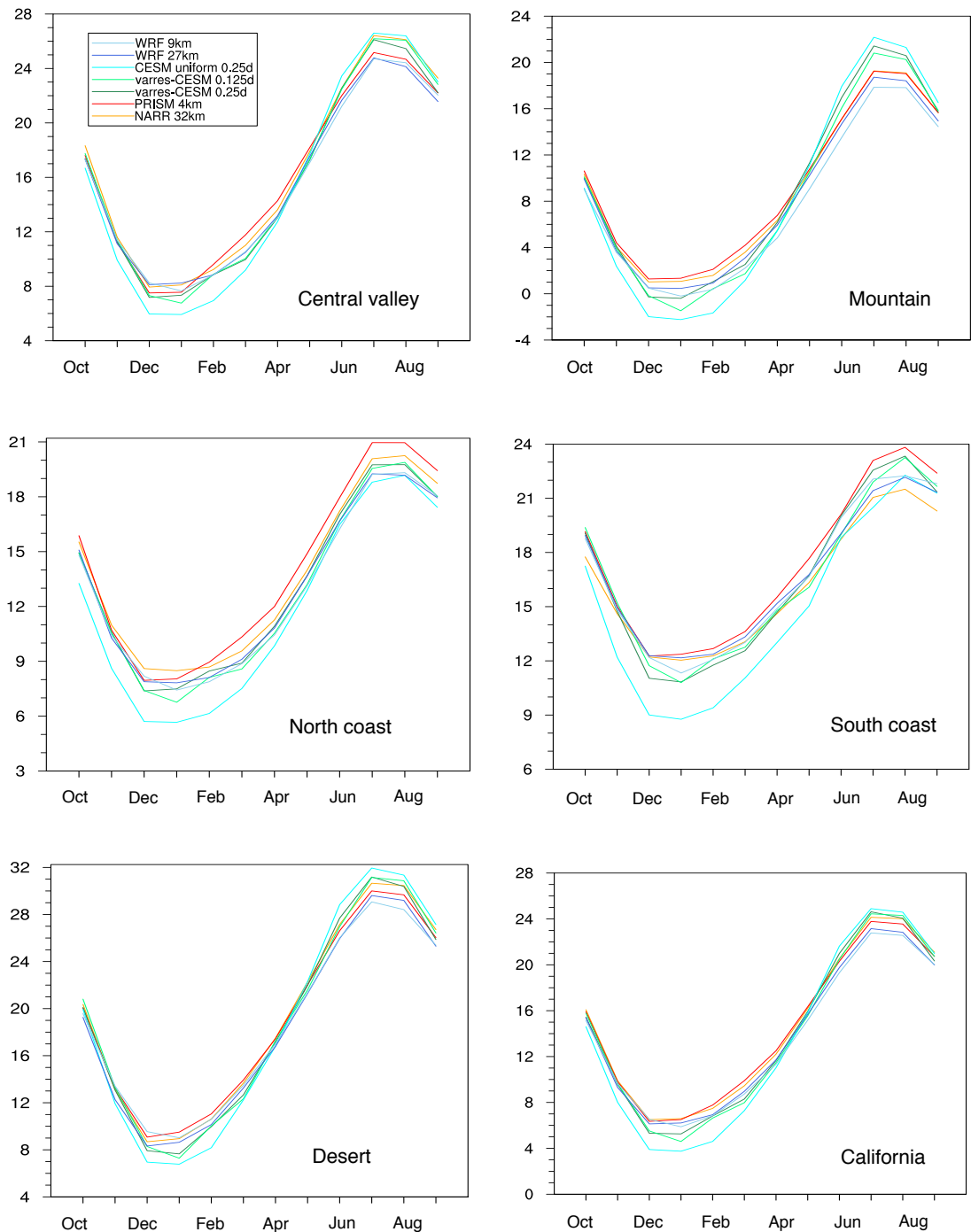
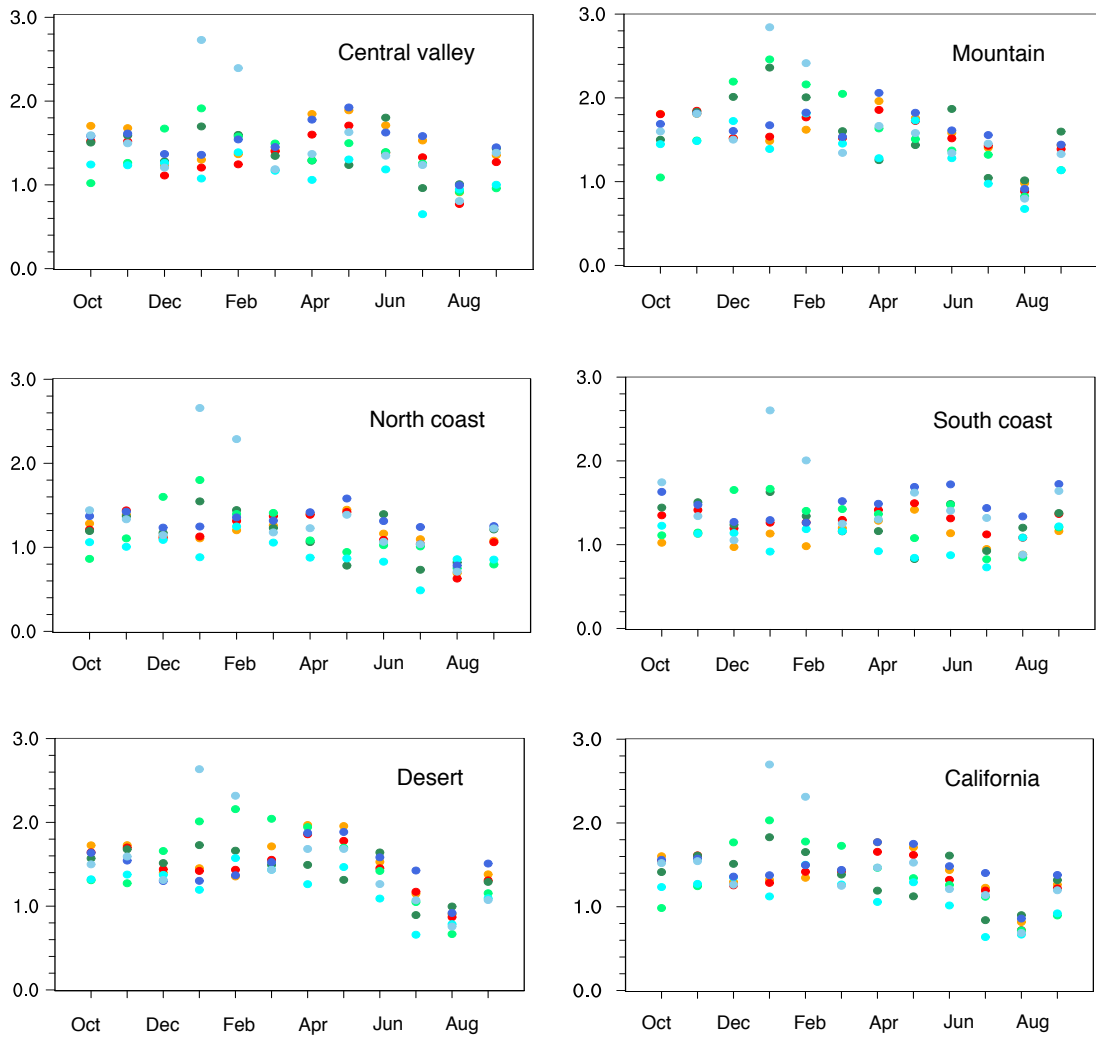


FIG. 5. sample standard deviation of JJA average daily Tmax, Tmin and Tavg from models and PRISM ($^{\circ}\text{C}$).



745 FIG. 6. Seasonal cycle of monthly-average Tavg for each subzone (°C). Bars represent standard deviation (σ)
746 values.



747 FIG. 7. Seasonal standard deviation (s) values of monthly-average T_{avg} for each subzone ($^{\circ}C$). Bars represent
748 standard deviation (s) values.

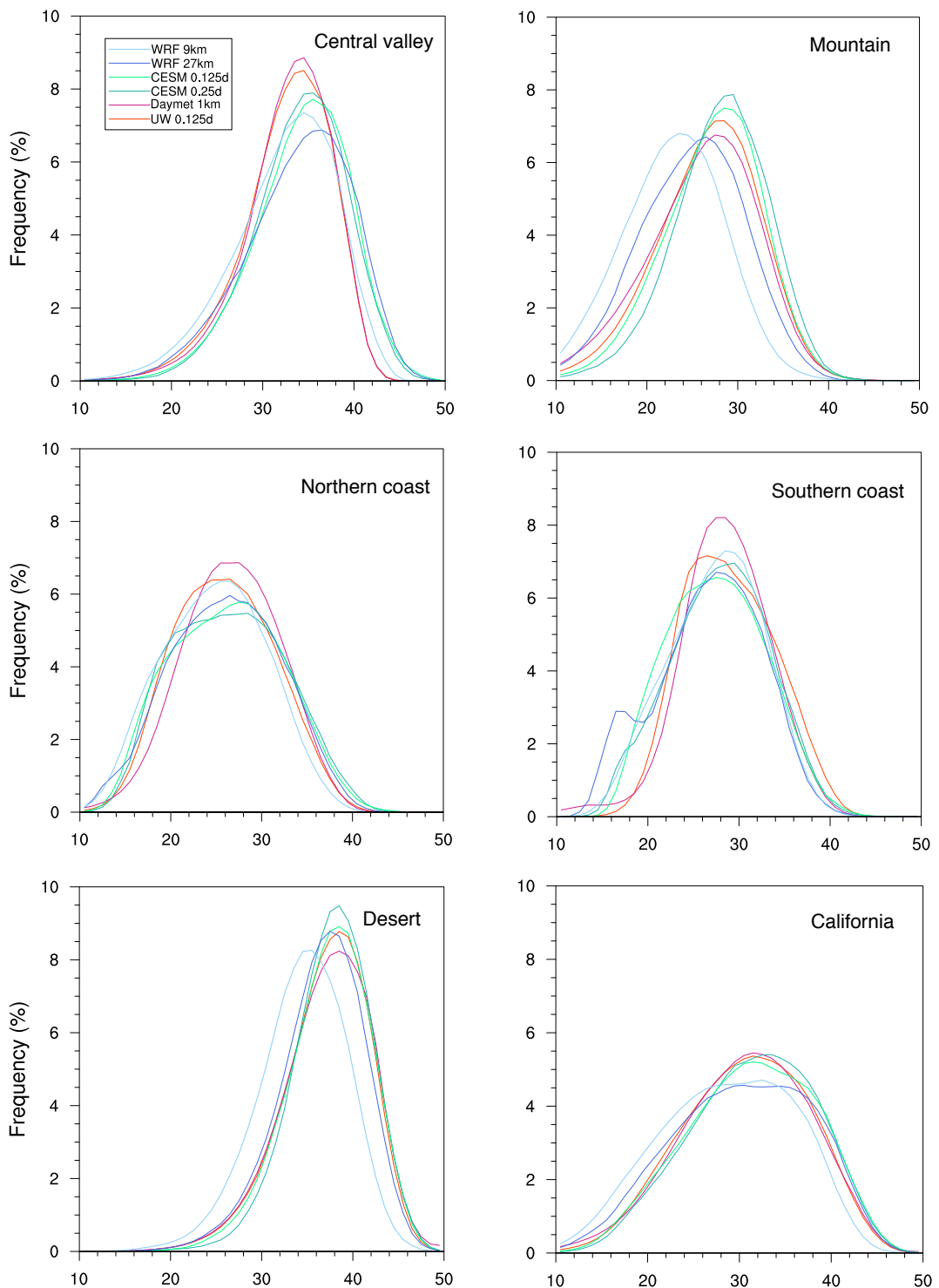


FIG. 8. Frequency distribution of summer Tmax ($^{\circ}\text{C}$).

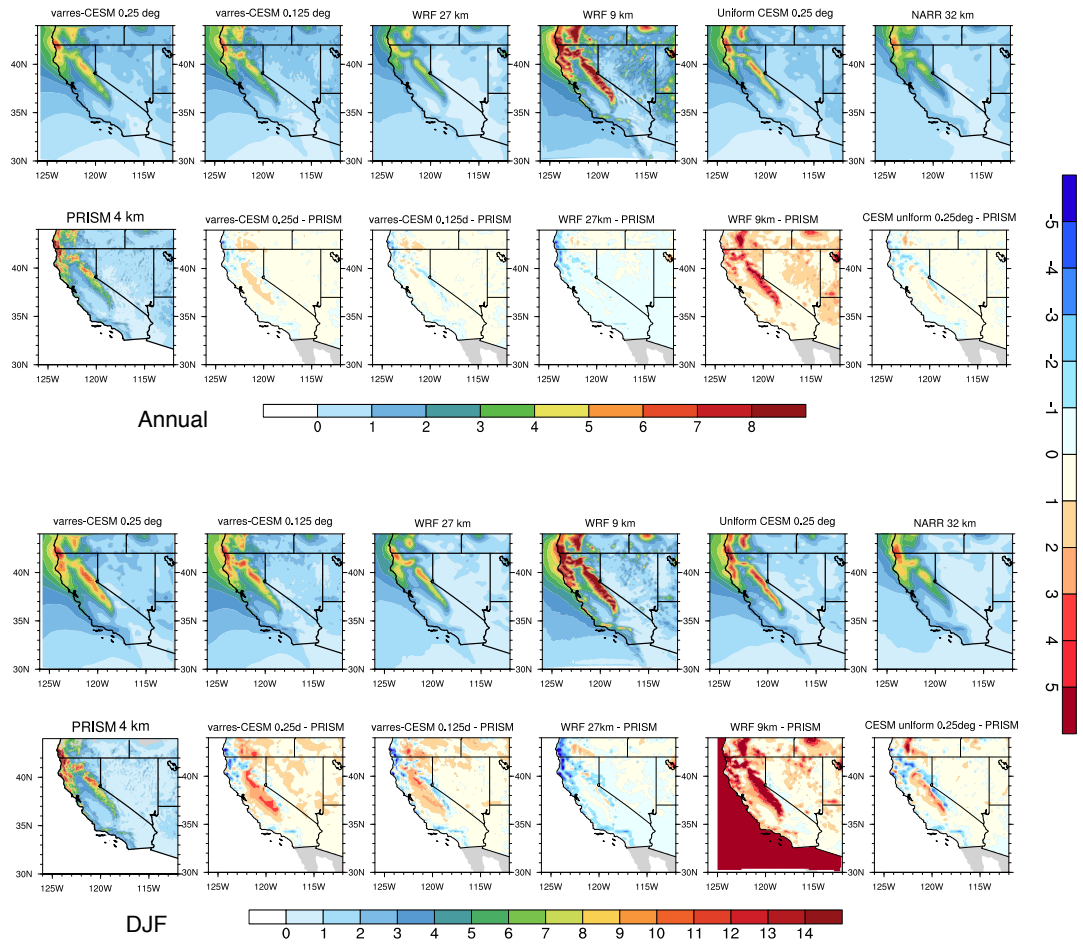


FIG. 9. Annual and DJF precipitation from models and reference datasets (mm/d).

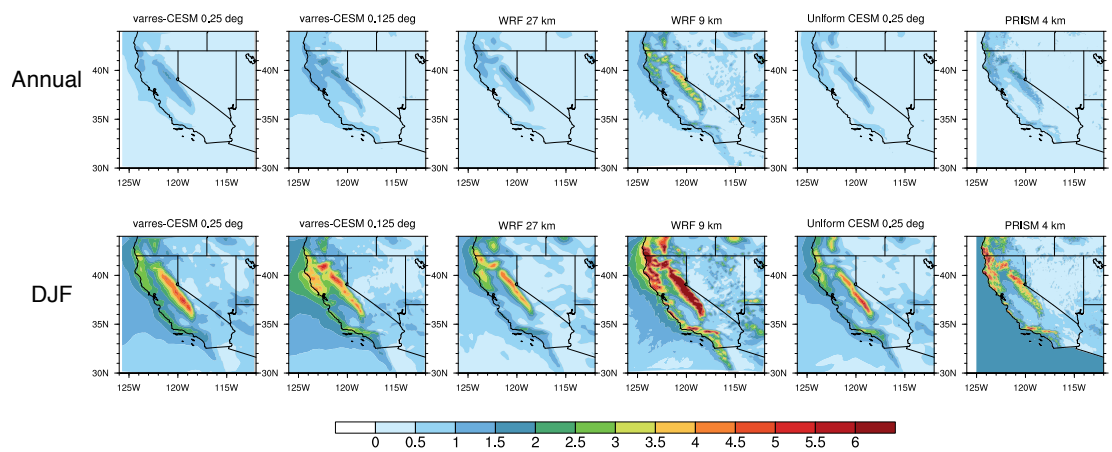


FIG. 10. sample standard deviation of Annual and DJF precipitation from models and PRISM (mm/d).

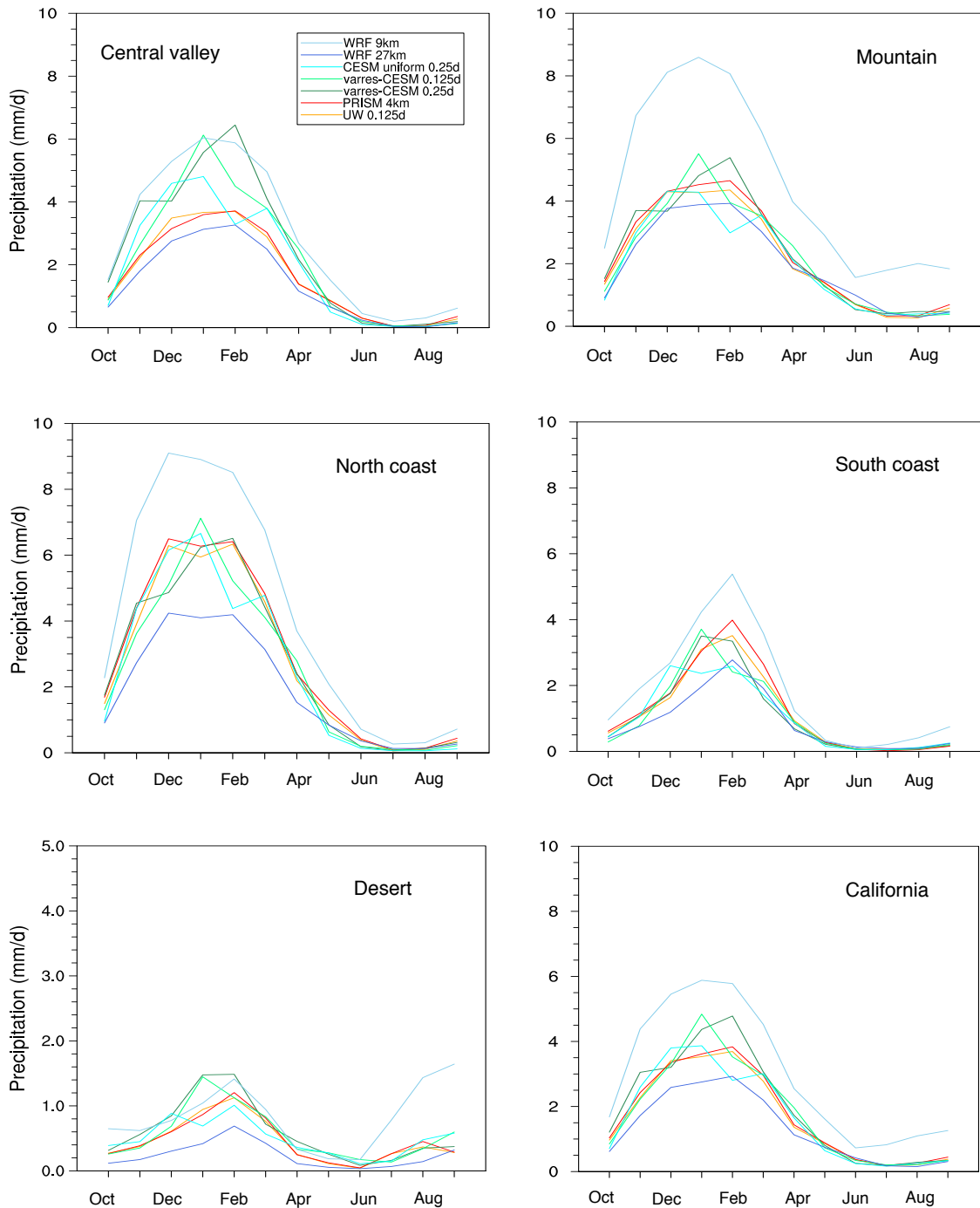


FIG. 11. As Figure 6, but for monthly-average total precipitation (mm/d).

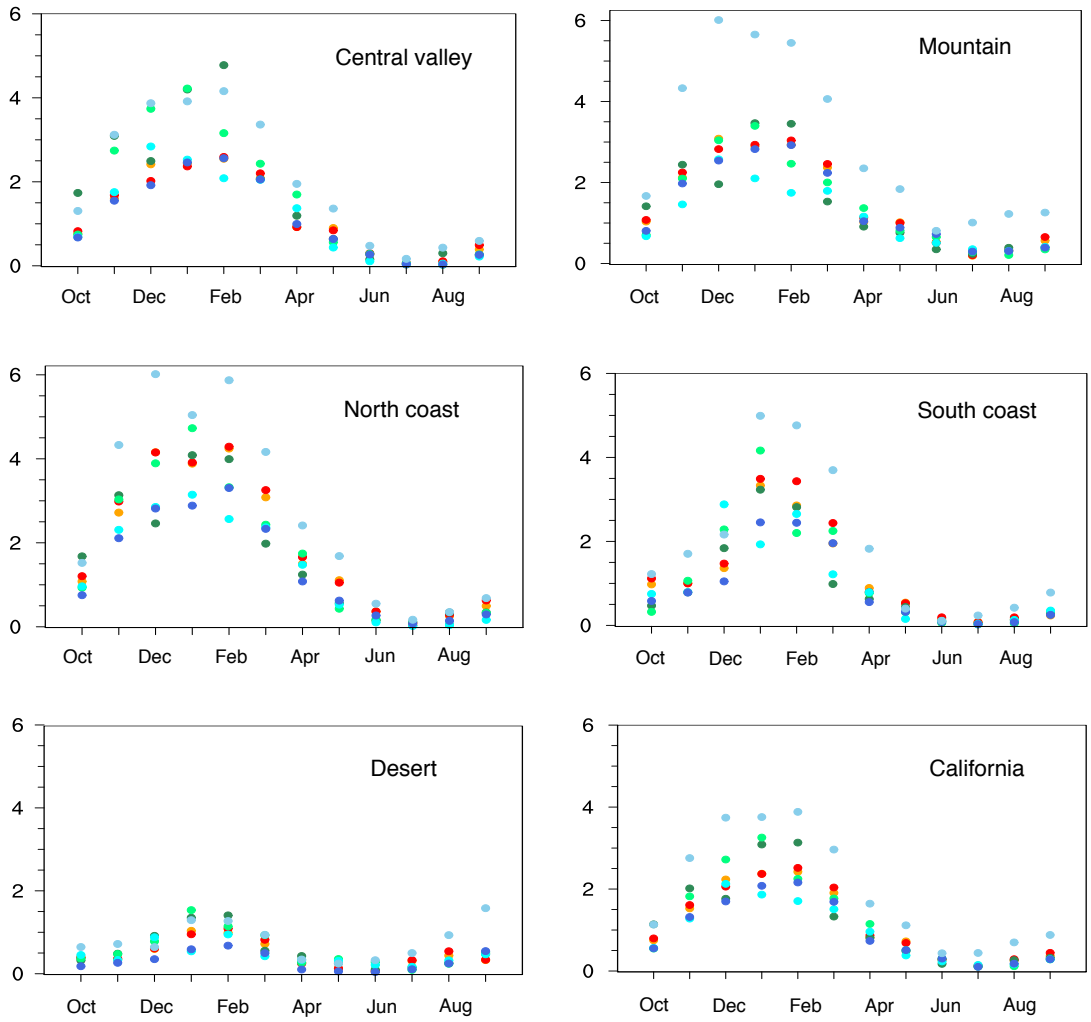
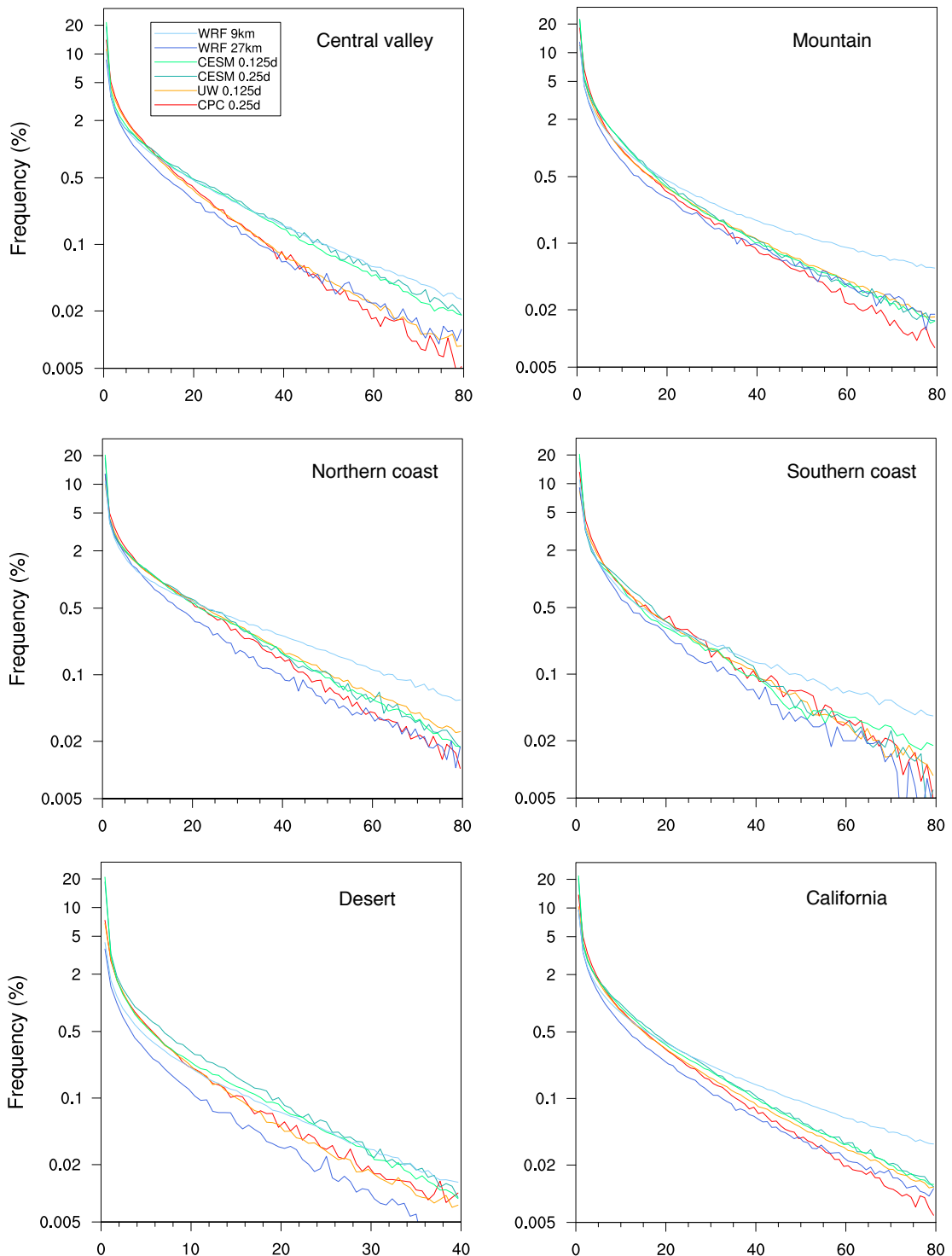
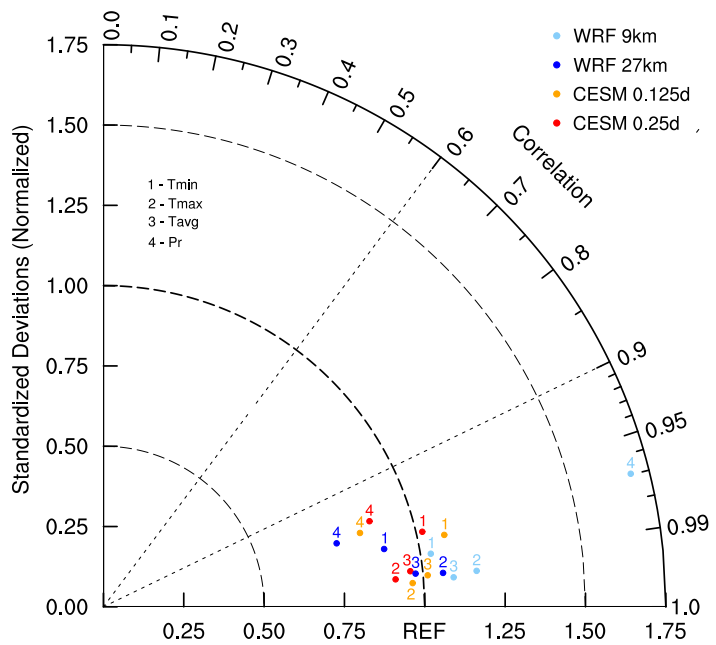


FIG. 12. As Figure 7, but for monthly-average total precipitation (mm/d).



749 FIG. 13. Frequency distribution of winter Pr constructed from 26 years of daily data (mm/d) (note that the
 750 vertical scale is logarithmic).



751 FIG. 14. Taylor diagram of annual climatology for the entire California region, using the PRISM dataset as
 752 reference.